Finite element based micro modelling of masonry walls subjected to fire exposure: framework validation and structural implications

P. Ravi Prakash[1], Miguel Azenha, João M. Pereira, Paulo B. Lourenço

Institute for Sustainability and Innovation in Structural Engineering (ISISE), University of Minho, Portugal

Abstract

This paper presents a 2-D finite element (FE) based micro modelling framework for thermo-mechanical response history analysis of solid brick masonry structures subjected to fire. The 2-D FE framework considers geometric and material nonlinearities, and transient states of strain in conjunction with the temperature-dependent material properties. Material nonlinearity within the 2-D FE model is considered by the temperature-dependent total strain rotating crack model. The FE framework is validated against the thermo-mechanical response of a half-scale masonry wall subjected to one-sided fire exposure, and it is observed that the predictions of the FE framework are reasonably accurate. Utilizing the validated FE framework, thermo-mechanical response history characterization is performed on a full-scale masonry wall subjected to one-sided fire exposure. Critical physical phenomena which include thermal bowing, heat diffusion, unit-mortar thermo-mechanical interaction, cracking and stress profiles within the masonry structures are studied intricately. Furthermore, thermo-mechanics within representative volumes enclosing unit as well as mortar and their correlation with the global thermo-mechanical response is studied. Such 2-D micro-scale thermo-mechanical computations on masonry walls followed by a detailed discussion on their thermo-mechanics are one of the novel features of the present study. It is

Email addresses: patnayakuni.prakash@civil.uminho.pt (P. Ravi Prakash), miguel.azenha@civil.uminho.pt (Miguel Azenha), jpereira@civil.uminho.pt (João M. Pereira), pbl@civil.uminho.pt (Paulo B. Lourenço)

[1]Corresponding Author

observed that thermal bowing resulted from a complex interaction between thermal dilation and cracking and crushing in the mortar and unit within the masonry structure.

Keywords: Thermo-mechanical analysis, Masonry, Fire resistance, Nonlinear thermal gradients.

1 Introduction

Ancient and modern infrastructural utilities employ masonry as one of the predominant material for structural and/or non-structural elements attributing to its excellent thermal, mechanical and acoustic properties. The response of such masonry structures has been well studied in the context of static and dynamic loading scenarios [1,2]. However, limited rather scarce understanding is available in the literature in the context of masonry structures subjected to fire exposure [3]. The design of masonry structures subjected to fire is usually done by the fire resistance rating quantification, which is essentially the time required by the structure for attaining the prescribed failure limit state which is usually in terms of strength, integrity and deflection limits [4]. The fire resistance ratings of masonry structures are normally evaluated by a) experimental methods [3], b) codified approaches (e.g. EN 1996-1-2 [4] and ACI 216.1-07 [5]) and c) numerical models (e.g. [6,7]).

Experimental methods involve the fire resistance rating quantification by exposing the masonry structure to a given fire scenario. The early experimental investigations on masonry subjected to fire include the full-scale fire tests on clay brick masonry walls conducted at the Experimental building station, Australia [8] to study the phenomenon of fire-induced thermal bowing. Lawrence and Gnanakrsihnan [9] conducted a comprehensive experimental investigation on clay brick masonry walls subjected to fire and quantified the effects of slenderness ratio and applied axial load on the overall thermo-mechanical behavior. Shields et al. [10] investigated the thermo-mechanical response of masonry walls subjected to the BS-476 fire exposure. Laverty et al. [11] tested scaled concrete brick masonry walls subjected to various load levels and fire exposures and had explained the phenomena of thermal bowing and reverse thermal bowing. Recently, Nguyen and Meftah [12] experimentally investigated the thermo-mechanical response of hollow clay block masonry walls subjected to fire exposure, and spalling was observed in their experimental investigation. Although such full-scale tests facilitate precise understanding of the thermo-mechanics of the masonry walls, they cannot be performed regularly for the prescriptive and/or performance based design of masonry walls subjected to fire due to the explicit costs and time involved in such tests.

Codified approaches essentially involve fire resistance rating quantification of masonry walls from the tabulated data available in the building codes (e.g. EN 1996-1-2 [13], IS-1642 [14] and ACI 216.1-07 [5]) as a function of the wall thickness. However, such an approach is prescriptive in nature and does not account for critical phenomena which may significantly influence the thermo-mechanics of the masonry wall like load level, geometric effects, boundary conditions and realistic fire exposures. These limitations can be alleviated with the aid of experimentally validated numerical models. Very limited numerical investigations have been performed on the numerical simulation of the thermo-mechanical response of the masonry structures subjected to fire. An early numerical model developed in this context includes the 2-D finite element (FE) model developed by Dhansekaran et al. [6]. Their FE model demonstrated thermal bowing in masonry walls and it is essentially a layered shell element which performs time-variant mechanical analysis with thermal gradients and temperature-dependent mechanical properties as input. Nadjai et al. [15] developed a 2-D FE based micro model for nonlinear thermo-mechanical analysis of masonry walls and successfully implemented in MasSET programme [16]. Their 2-D FE model accounts for geometric and material nonlinearities, thermal gradients, temperature-dependent material properties and transient states of strain. Later, they had demonstrated applications pertaining to the behavior of compartmental masonry walls subjected to fire exposure [17] using their MasSET programme. Nguyen and Meftah [18] demonstrated a numerical validation study on a hollow clay block masonry subjected to fire exposure utilizing a nonlinear 3-D FE micro modelling approach in Cast3M. To model the observed spalling in the experiment, their numerical model considered a crushing-detachment-buckling based spalling criteria and was successfully validated against the experimental observations. Recently, Kumar and Srivastava [19] had demonstrated the effect of masonry infill on the in-plane and out of plane response of the fire exposed masonry in-filled reinforced concrete frame utilizing a nonlinear 3-D FE simplified micro model in ANSYS. Their numerical investigation indicated a significant influence of masonry on the overall stability of the masonry in-filled RC frame at elevated temperatures.

Aforementioned works pertaining to the numerical modelling of masonry structures provide a perspective on the thermo-mechanical response of masonry walls subjected to fire. However, masonry being a complex material with different thermal and mechanical properties of the constituents, a detailed understanding is needed on the unit level thermo-mechanics and its correlation with the global thermo-mechanical response. Such a discussion is observed to be missing in the present literature and is the prime focus of the present study. This study demonstrates an intricate numerical investigation on masonry walls subjected to fire utilizing a 2-D FE micro model in DIANA-FEA [20]. The unit and mortar are modelled separately within the 2-D FE model and it accounts for a) geometric and material nonlinearities, b) nonlinear thermal gradients, c) temperature-dependent mechanical and thermal properties, d) cracking and crushing of materials, and e) transient states of strain.

The present paper is organized as follows. Section 2 presents the theoretical aspects of the 2-D FE modelling based simulation framework which include assumptions, thermo-mechanical components of the FE model, and temperature-dependent material models. Next, Section 3 presents the experimental validation study pertaining to half-scale masonry wall subjected to fire exposure. Section 4 demonstrates a scenario based thermo-mechanical analysis of full-scale masonry wall subjected to fire exposure. Finally, Section 5 concludes the present study.

2 Simulation framework

This study utilizes a nonlinear 2-D FE micro modelling based framework to evaluate the thermo mechanical behaviour of solid brick masonry walls subjected to fire. The framework is formulated in a plane stress setting assuming a uniform fire exposure and mechanical boundary conditions along the top and bottom surfaces of the wall. In the case of thermal analysis, such an approach is considered ideal as no lateral conduction is expected for such a uniform fire exposure. However, in the case of mechanical analysis such plane stress approach may not be ideal in case of walls with complete or partial lateral restraint (in the direction perpendicular to the 2D simulation plane). Moreover, the unit-joint thermo-mechanical interactions along the lateral direction are ignored. Such a 2-D framework with above mentioned plane stress idealization facilitates computationally efficient thermo-mechanical analysis of masonry walls subjected to fire. However, in scenarios involving a deviation of the aforementioned assumption, 3-D FE modelling should be preferred. Furthermore, the developed framework in its present form is not applicable for the thermo-mechanical analysis of hollow-brick masonry walls.

It is to be noted that FE based computational modelling of masonry is usually done utilizing micro and macro based modelling strategies, respectively [2]. Within the micro modelling, which is the main focus of the present study, three approaches are possible, namely: a) detailed micro modelling, b) continuum micro modelling, and c) simplified micro modelling (Figure 1). In the case of detailed micro modelling, the unit, mortar and the unit-mortar interface are modelled separately. Continuum micro modelling is a simplified version of detailed micro modelling strategy, with bonded interfaces. In the case of simplified micro modelling strategy, unit and mortar are modelled together as a composite unit with interface elements at the half thickness of the mortar. These approaches have their own merits and de-merits and have been a matter of discussion among various researchers (e.g. Lourenço [2] and Mohyeddin [21]). In the context of thermo-mechanical modelling of masonry exposed to fire, detailed micro modelling strategy facilitates precise modelling of physical phenomena and is capable of considering localized failure modes (cracking, crushing and various modes of fracture at the unit-mortar interface).

However, at elevated temperatures, the temperature-dependent mechanical behavior of the unit-mortar interface is still not established due to the lack of comprehensive experimental research, specifically targeted to the temperature-dependency of the nonlinear interface behavior.

This limitation can be partly alleviated by extending the temperature-dependency in mechanical properties of cement mortar to the unit-mortar interface. However, detailed model calibration studies are required to account for the lack of experimental data pertaining to the temperature-dependent coupled tension-shear failure mode in cement mortar [22] . Furthermore, convergence issues are expected due to the complex temperature-dependent interface nonlinearity. In view of such complex limitations, the present study models unit and mortar separately in a combined geometric and material nonlinearity setting using the continuum micro modelling strategy. Although such approach does not account for temperature-dependent interface behaviour, it accounts for the localized failures expected in the mortar joints as well as units and such approach has been successfully implemented in the past as well (e.g. [15,18]). Utilizing the aforementioned modelling strategy in the considered framework, the thermo-mechanical response histories of masonry walls are demonstrated in the present study.

Figure 2 shows the 2-D FE model which performs thermo-mechanical analysis with various thermal and mechanical boundary conditions. The thermo-mechanical analysis is performed utilizing a staggered one-way coupling scheme. In such a scheme, the thermal analysis is performed first on a fixed geometry followed by time-variant mechanical analysis at constant temperatures corresponding to various time steps [23]. Such a scheme is computationally efficient unlike the theoretically precise monolithic schemes [23] which might lead to a large system of equations with asymmetry and eventually makes the analysis computationally very intensive. In the context of the present simulation framework, the need for a fully coupled strategy has been demonstrated to be of relatively small importance, hence the staggered analysis strategy is chosen. The theoretical aspects of the individual thermal and mechanical FE models are discussed in Sections 2.1 and 2.2 respectively.

2.1 Thermal FE model

For a 2-D body as shown in Figure 2, the heat transfer is governed by conduction, convection and radiation. Within the 2-D solid body enclosed by $\mathbf{\Omega}$, heat transfer is governed by thermal conduction, whereas the heat transfer from the heating source to the exposed boundaries is governed by convection and radiation. The governing equation to model the heat transfer is deduced from the law of energy balance and is given by

$$(\rho c)_T \frac{\partial T}{\partial t} = \nabla.(\boldsymbol{\gamma}_T \nabla T), \tag{1}$$

where $(\rho c)_T$ represents temperature-dependent specific heat capacity, T represents temperature, $\boldsymbol{\gamma}_T$ represents temperature-dependent thermal conductivity tensor. It is to be noted that the external fire temperature is applied either as Dirichlet or Neuman boundary condition (convection and radiation). The governing equations for the convection and radiation on the boundary $\boldsymbol{\Gamma}_\mathbf{N}$ are given by

$$\begin{aligned}(\boldsymbol{\gamma}\nabla T).\mathbf{n} &= -h_c\left(T - T_f\right),\\ (\boldsymbol{\gamma}\nabla T).\mathbf{n} &= -h_r\left[\left(T + 273.15\right)^4 - \left(T_f + 273.15\right)^4\right],\end{aligned} \tag{1}$$

where T_f represents the fire temperature, h_c represents the convective heat transfer coefficient, h_r ($h_r = \chi\zeta\xi$) represents the radiative heat transfer coefficient, χ represents the form factor, ζ represents the emissivity, and ξ represents the Stefan-Boltzmann constant (5.678×10^{-8}W/m^{2}K^4). Ritz-Galerkin FE discretization is applied to Equation (1) utilizing the eight-node quad element and two-node line element as shown in Figure 2. The eight-node quad element work on the solid body enclosed by $\boldsymbol{\Omega}$**,** and with four integration points in a full integration setting**.** Whereas the two-node line element work on the boundary convection and radiation at the $\boldsymbol{\Gamma}_\mathbf{N}$, and with two integration points in a full integration setting. Upon discretization, a system of equations is obtained as [24]

$$\mathbf{M}\dot{\mathbf{T}}(t) + \mathbf{K}\mathbf{T}(t) = \boldsymbol{\psi}(t), \tag{2}$$

where $\mathbf{M}$ represents the heat capacity matrix, $\mathbf{K}$ represents the conductivity matrix and $\boldsymbol{\psi}(t)$ represents the heat load vector. These systems of equations are highly nonlinear in nature due to temperature-dependent material properties and boundary conditions and are solved iteratively using the Newton-Raphson method until the L_2 norm of temperature reaches the prescribed value of tolerance.

2.2 Mechanical FE model

For the 2-D FE model as shown in Figure 2, the time-variant mechanical analysis component is executed in a one-way coupling scheme, with the temperature history of the previously executed thermal analysis as an input. For the 2-D body enclosed by $\mathbf{\Omega}$, the Galerkin FE discretization is applied using 8-node quad element with four integration points in a full integration setting. Subsequently, the incremental equilibrium equations are obtained as

$$\mathbf{K}\Delta\mathbf{d} = \Delta\mathbf{F}_{\mathrm{m}} + \Delta\mathbf{F}_{\mathrm{th}}, \tag{3}$$

where $\mathbf{K}$ represents the temperature-dependent element stiffness matrix derived in a total Lagrangian based formulation, $\Delta\mathbf{d}$ represents the element displacement vector, $\Delta\mathbf{F}_{\mathrm{m}}$ represents the incremental force vector pertaining to mechanical loading, and $\Delta\mathbf{F}_{\mathrm{th}}$ represents the incremental force vector pertaining to thermal effects. The incremental system of equations shown in Equation (4) are derived from the principle of virtual work [24] in conjunction with temperature-dependent constitutive relation $\left(\boldsymbol{\sigma} = \mathbf{D}_T\left(\boldsymbol{\varepsilon} - \boldsymbol{\varepsilon}_{\mathrm{T}}\right)\right)$. Wherein, $\boldsymbol{\sigma}$ represents the second Piola-Kirchhoff tensor, $\mathbf{D}_T$ represents the temperature-dependent constitutive matrix, $\boldsymbol{\varepsilon}$ represents the total Green-Lagrange strain, $\boldsymbol{\varepsilon}_{\mathrm{T}}$ represents the total thermal strain. A detailed description of the strain components and the constitutive matrix will be discussed subsequently. Equation (4) is highly nonlinear in nature and is solved iteratively. In the present study, the Newton-Raphson based nonlinear solution strategy is followed with a prescribed tolerance value of 0.001 on the L_2 norms of energy.

2.3 Material models

This section illustrates the temperature-dependent material models used within the 2-D FE modelling based simulation framework. In the context of thermal analysis, the temperature-dependency in $(\rho c)_T$ and $\boldsymbol{\gamma}_T$ in the context of thermo-mechanical modelling of masonry walls will be discussed in the respective numerical simulation sections, respectively. The total Green-Lagrange strain ($\boldsymbol{\varepsilon}$) discussed in Section 2.2 is decomposed as

$$\begin{aligned} \boldsymbol{\varepsilon} &= \boldsymbol{\varepsilon}_{\mathrm{m}} + \boldsymbol{\varepsilon}_T, \\ \boldsymbol{\varepsilon}_T &= \boldsymbol{\varepsilon}_{\mathrm{th}} + \boldsymbol{\varepsilon}_{\mathrm{tc}}, \end{aligned} \tag{4}$$

where $\boldsymbol{\varepsilon}_{\mathrm{m}}$, $\boldsymbol{\varepsilon}_{\mathrm{th}}$ and $\boldsymbol{\varepsilon}_{\mathrm{tc}}$ represent mechanical strain, total thermal strain, thermal strain and transient creep strains, respectively. A perspective on the additive decomposition of concrete strains under transient thermal conditions can be seen in [25,26]. The thermal strain is computed as

$$\boldsymbol{\varepsilon}_{\mathrm{th}} = \alpha_T \Delta T, \tag{5}$$

where α_T is the temperature-dependent coefficient of thermal expansion. The transient creep strain in the present FE model, the transient creep strain is modelled using the empirical relationship proposed by Anderberg and Thelanderson [27] as

$$\Delta\boldsymbol{\varepsilon}_{\mathrm{tc}} = \tau \left(\frac{\sigma}{f_{c,20}} \right) \Delta\boldsymbol{\varepsilon}_{\mathrm{th}}, \tag{6}$$

where σ represents stress at a given time, $f_{c,20}$ represents the compressive strength of concrete at 20 °C and τ is constant which ranges between 1.8 and 2.5. Further, details of the transient creep strain in the context of the present study will be explained in the respective numerical simulation sections. It is to be noted that the standard creep is not considered in combination with the transient creep in the simulation framework, as the considered time scales are very small eventually resulting negligible contribution from the standard creep [27]. The mechanical strain is governed by the temperature-dependent constitutive relation $\left(\boldsymbol{\sigma} = \mathbf{D}_T\left(\boldsymbol{\varepsilon} - \boldsymbol{\varepsilon}_{\mathrm{T}}\right)\right)$ and is computed using the total strain rotating crack model. Consideration of rotating crack model instead of a fixed crack model has been a matter of discussion among various researchers after it was first introduced by Cope et al. [28]. In the fixed crack model, the material axes of symmetry are fixed throughout the analysis and it may result in inaccurate model predictions in scenarios involving a change in the principal directions during the course of loading [29]. This limitation has been circumvented with the aid of rotating crack model, where the misalignment between the principal directions and principal axes of symmetry is adjusted by co-rotating the principal axes of symmetry. In a total strain rotating crack model based constitutive framework, the temperature-dependent constitutive matrix ($\mathbf{D}_T$) is computed from the 1-D temperature-dependent inelastic constitutive relations (Figure 3) in the tensile and compressive regimes, respectively. The background theory for such numerical implementation can be seen in [28,30] and not repeated here for the sake of brevity.

In case of tension regime, the 1-D inelastic constitutive relation is elastic with linear softening as shown in Figure 3 and is characterized by the temperature-dependent tensile strength ($f_{t,T}$) and fracture energy corresponding to mode-1 ($G_{f1,T}$). The temperature dependency of above mentioned parameters in the context of the present study will be discussed in the respective numerical simulation studies. In the case of compression regime, a parabolic curve with linear softening as in EN1992-1-2 [31] is considered for 1-D inelastic constitutive relation and is characterized by temperature-dependent compressive strength ($f_{c,T}$), strain at peak compressive strength ($\varepsilon_{cp,T}$) and ultimate compressive strain ($\varepsilon_{cu,T}$).

3 Simulation of the experiment of half-scale masonry subjected to fire

The accuracy of the 2-D FE based simulation framework is established by validating the experimental investigation of Laverty et al. [11]. Their experimental study essentially involves a half-scale masonry wall (b=430 mm; h=1330 mm; t=50 mm) subjected to one-sided fire exposure as shown in Figure 4. The half-scale wall is built with concrete bricks (100×32×50 mm) with 20 MPa compressive strength, bedded on 1:3 cement-sand mortar mix (5 mm thick) pertaining to ordinary Portland cement. The wall is rested on a firm steel base and an axial load of 50 kN, which is 50% of the design ultimate load is applied on the wall through the steel plate, which is restrained against lateral translation as shown in Figure 4. The temperatures were measured at the central vertical third positions (h/3 and 2h/3) of the wall at various depths (0, t/6, t/2, 5t/6 and t) along the cross-section, whereas the lateral deflections were measured at the mid-span, top and bottom, respectively. Utilizing the simulation framework, thermo-mechanical analysis is performed with the mesh-size shown in Figure 4. The chosen mesh size is based on mesh convergence studies.

To quantify the effect of temperature-dependent material nonlinearity, the analysis is also performed in a thermo-elastic setting with temperature-dependent thermal and mechanical properties. It is to be noted that in the present simulation framework, geometric effects which include large deformations, large rotations and large strains are modelled by the total Lagrangian formulation (TLF) [32]. To quantify the effect of large strains, additional thermo-mechanical analysis is performed without considering the geometric effects. The wall is fixed at the base and restrained against lateral translation at the top as shown in Figure 4. The mechanical load is applied with the aid of a steel plate, and such loading is simulated by modelling steel plate separately with a line interface between steel plate and wall (K_n= 56 kN/m^3; K_t =5.6 kN/m^3) and the tensile strength of the interface is taken as zero. Such values are chosen from the elastic material properties of the steel plate in conjunction with the mesh characteristics.

3.1 Material properties

The material properties utilized for validating the aforementioned experimental investigation in the context of present 2-D FE framework is presented herein. A summary of these properties at room temperature (T=20 °C) is shown in Table 1.

The temperature-dependency in specific heat capacity and thermal conductivities of concrete unit and cement mortar are taken from the EN1992-1-2 [31] and are shown in Figure 5. It should be noted that there is no specific mention of aforementioned thermal properties in the experimental investigation of Laverty et al [11]. The properties from EN1992-1-2 [31] have been chosen as they explicitly account for the latent heat effects pertaining to the inherent moisture within the masonry wall. A moisture content of 3% by weight is assumed in the present validation study. As will be shown subsequently, the chosen thermal properties resulted in reasonably accurate thermal histories. The temperature-dependent thermal expansion coefficient for concrete unit as well as cement mortar are taken from the EN1992-1-2 [31] corresponding to that of calcareous aggregates.

The coefficient τ pertaining to the transient creep strain is taken as 2.0 for both concrete unit and cement mortar, and such value has been ascertained from the parametric studies. The required material properties pertaining to the rotating crack constitutive framework discussed in Section 2.3, at T =20 °C are taken from the studies of Laverty et al. [11,15]. It is to be noted that the temperature-dependency in aforementioned mechanical properties is taken from EN1992-1-2 [31]. This is attributed to their predominate applications by the fire engineering community as well as the lack of comprehensive experimental investigation pertaining to the constituent materials of the half-scale test. The temperature-dependency in compressive and tensile strengths of concrete unit and cement mortar is shown in Figure 6. The temperature-dependency in $\varepsilon_{cp,T}$ and $\varepsilon_{cu,T}$ of concrete unit and cement mortar is shown in Figure 7. Further, the temperature-dependent mode-1 fracture energy of concrete unit and cement mortar are computed from the empirical relation provided by FIB model code [33], which is written as

$$G_{f1} = 73 f_c^{0.18}. \tag{7}$$

3.2 Results and discussion

A comparison of thermal and mechanical (out of plane deflection) response histories of the half-scale masonry wall is shown in Figure 8, for both the elastic and inelastic cases. The temperature histories at the designated locations shown in Figure 4 are in good agreement with their experimental counter parts with maximum error of 3.14%. The mechanical deflection history is in reasonably good agreement with the experimentally observed values with failure time corresponding to 23 min (numerical failure), whereas the experimentally observed failure time is 28 min. The elastic mechanical response history is imprecise in comparison to the experimentally observed values, although it demonstrates thermal bowing. The effect of geometric nonlinearity on the thermo-mechanical response history is shown in Figure 9. It is observed that the mechanical (out of plane deflection) response history is inaccurate with reference to the experimentally observed values, when the geometric effects are not considered. Also, reverse thermal bowing is observed unlike in the experiment as well as the geometric nonlinear simulation, which is due to the temperature-dependent material degradation and damage. Furthermore, the results indicate the importance of consideration of geometric effects in the purview of present simula-tion framework. The mechanical response history of the central line of the wall is shown in Figure 10. This response indicates thermal-bowing of the wall and its amplification at the verge of failure. The response of masonry wall subjected to fire is governed by the combined effects of nonlinear thermal gradients, geometric effects, applied load, boundary conditions and temperature-dependent material degradation.

A discussion on these phenomena in the context of the masonry wall under consideration and their contribution to the mechanical response history is explained herein. Figure 11 and Figure 12, show the thermo-mechanical response of the wall under consideration at t= 5 min and t=23 min, respectively.

It shoud be mentioned that tensile stresses are considered positive, whereas the compressive stress are considered negative and such notation is followed over the entire paper. Firstly, the results at t=5 min indicate temperature-diffusion across the wall which eventually resulted in nonlinear thermal gradients across the wall thickness and overall thermal expansion of the wall. It is to be noted that, in the process of attaining a quasi-static equilibrium, such nonlinear thermal gradients result in additional stresses in masonry wall which are compressive in the heated zone and tensile in the adjacent non-heated zone. However, the nature of theses stress states are further influenced by the applied mechanical load and boundary conditions.

For instance, the presence of a fixed base and a hinged boundary condition at the top of the wall under consideration resulted in an additional temperature-induced restraint stresses which are compressive in the heated zone and tensile in the non-heated zone. The influence of these restraint stresses are evident near the fixed base (see σ_{yy}, Figure 11).

Such a combined stress state resulting from thermal dilation and mechanical boundary conditions resulted in a thermal-bowing profile as shown in Figure 10. Further, no cracking was observed in the wall upto t=5 min. However, after further fire exposure, the thermal diffusion accelerates and the stress states are predominantly influenced by temperature-dependent material degradation in conjunction with cracking and crushing. This can be seen in the thermo-mechanical response at t=23 min (Figure 12), where one can see the predominant tensile zone that induced cracking at the base. Further, such localized cracking significantly influenced the overall mechanical response of the structure and this is explained herein with the aid of thermo-mechanical response histories of representative volume units (RVU) taken at heights of 0.66m (Figure 13) and 0 m (Figure 14) from the base, respectively.

Moreover, the stress (σ_{yy}) histories at the designated locations , labelled as M_A, M_B and M_C (see Figure 13) in the aforementioned RVUs are shown in Figure 15. During initial stages of fire exposure, in the case of RVU-1, the observed stress states (see Figure 13, t=5 min) are governed by the thermal gradients as well as the fire induced restraint stress due to the fixed base. This resulted in an increase in the compressive stress in the heated zone (Figure 15, RVU-1, M_A) and reduction in the compressive stress in the adjacent non-heated zone (Figure 15, RVU-1, M_B). Whereas in the case of RVU-2, an increase in in the compressive stress in the heated zone (Figure

15, RVU-2, M_A) and reduction in the compressive stress in the non-heated zone (Figure 15, RVU-2, M_B & M_C) are observed.

However, the increase is higher compared to RVU-1 and is attributed to the predominance of fire induced restraint stresses at the base. After further fire exposure, a shift of the compressive zone is observed in case of RVU-1 towards the unexposed face (See Figure 13, σ_{yy}).

This is characterized by a reduction in compressive stresses in the heated zone (Figure 15, RVU-1, M_A) and an increase in compressive stress in the adjacent non-heated zone (Figure 15, RVU-1, M_B). This is attributed to the temperature-dependent material degradation in the heated zone in conjunction with the nonlinear thermal gradients arising due to further heat diffusion.

Whereas in the case of RVU-2, cracking is initiated at the base and an increase in the cracking zone is observed with further fire exposure (Figure 14, Normal cracking stress). This is characterized by tensile stress histories in the non-heated zone (Figure 15, RVU-2, M_B & M_C). Furthermore, in the case of RVU-1, an increase in compressive stress is observed in the non-heated zone (Figure 15, RVU-1, M_C). This is attributed to excessive cracking and crushing at the base in RVU-2 (Figure 14, Normal cracking stress) and such cracking and crushing releases the tensile stresses originating from the base. At t=23 min, further cracking is observed in RVU-2 and resulted in the partial release of the rotational restraint at the base. This is characterized by a change in the stress-states in RVU-1 (Figure 13) and further resulted in the onset of large out of plane displacements (see Figure 10) and eventually the failure of the masonry wall. However, in the experimental investigation by Laverty et al. [11,15], on the half-scale masonry wall under consideration, detailed observations pertaining to the aforementioned cracking induced collapse were not taken. Laverty et al. [11,15] reported that the fire exposed side of the wall could not be seen due limitations specifically targeted to their scaled fire test.

3.3 Parametric studies

To quantify the effect of assumed parameters, as well as to demonstrate the accuracy of the developed FE framework, parametric studies are performed on the half-scale masonry wall. Figure 16a shows the parametric study on transient creep strain, where the coefficient τ (See section 2.3) is varied between 1.8 to 2.4. The results indicate that the increase in τ results in increase in the failure temperature and is due to the reduction in the total thermal strain. Figure 16b shows parametric study on the effect of initial tensile strength of mortar ($f_{t,20}$), where the tensile strength is varied between 0.8 to 1.2 MPa.

The results indicate slight increase in the failure temperature with increase in the tensile strength of mortar, with almost similar thermo-mechanical response history. Also, parametric study is performed on the temperature-dependency of the tensile strength of mortar and unit. The temperature-dependency as in Thelandersson [34] is compared to that of the EN1992-1-2 [31]. The thermo-mechanical response histories are observed to be similar in both the cases, with slightly higher failure temperature in the case of EN1992-1-2 [31].

4 Full-scale masonry wall subjected to ISO-834 fire exposure

Taking advantage of the previously discussed simulation framework, it was decided to study a different type of masonry wall. This full-scale wall is made of solid clay bricks and the arrangement of the bricks differs from the previous one. This full-scale masonry wall shown in Figure 18 is subjected to ISO-834 fire curve, which is also shown in the figure. The wall is loaded axially and is fixed at the base, and is free to translate and rotate at the top. The design axial load capacity of the wall is quantified in accordance with the EN1996-1-1 [35] and its corresponding fire resistance rating for 50% of the design axial load on the wall is observed to be 240 min from the EN1996-1-2. Thermo-mechanical analysis is performed using the 2-D FE based simulation framework with the mesh-size shown in Figure 18. As discussed in the case of half-scale masonry wall, thermo-elastic analysis is also performed with temperature-dependent thermal and mechanical properties. Axial load corresponding to 50% of the load-carrying capacity of wall is applied in the form of pressure at the top of the wall, which is 0.853 MPa.

4.1 Material properties

The material properties utilized for the full-scale masonry wall are presented herein. A summary of these properties at room temperature (T=20 °C) is shown in Table 2. In the case of cement mortar, the temperature-dependent thermal and mechanical properties are taken from Section 3.1. In the case of clay unit, the temperature-dependency in specific heat capacity and thermal conductivities of clay unit is taken from the EN1996-1-2 [13] and is shown in Figure 19.

Due to the lack of availability of comprehensive studies on the nature of transient creep strain in clay unit [36] , the transient creep component is ignored in the present numerical simulation. The temperature-dependent thermal expansion coefficient for the clay unit is taken from the EN1996-1-2 [13]. The temperature-dependent $f_{c,T}$, $\varepsilon_{cp,T}$ and $\varepsilon_{cu,T}$ are taken from EN1996-1-2 [13]. It is to be noted that the temperature-dependency of above mentioned parameters is shown up to 750 °C in EN1996-1-2 [13], and for higher temperatures beyond 750 °C, linear extrapolation is followed in the present study (see Figure 20 and Figure 21). In case of $f_{t,T}$, due to the lack of data (both experimental and code provisions), the temperature-dependency in $f_{t,T}$ is assumed to be the same as that of $f_{c,T}$.

The mode-1 fracture energy corresponding to room temperature is taken from the work of Lourenço et al. [37] and to it, the same temperature-dependency as in $f_{t,T}$ is applied, assuming a constant ductility index.

4.2 Results and discussion

The deformed configuration of the central line (scaling 10x) of the wall is shown in Figure 22a. The deformation history of top of the wall is shown in Figure 22b, for both the elastic and inelastic cases, respectively. Significant thermal bowing is observed and the rate of increase of thermal bowing is more predominant in the initial one hour. This is attributed to the nature of the ISO-834 fire curve coupled with lower thermal conductivities of unit and mortar, which eventually resulted in higher thermal increments during the initial one hour of fire exposure. However, no reverse thermal bowing was observed for the masonry wall. It is to be noted that the deformation histories are similar for both the elastic and inelastic cases, respectively unlike the half scale wall.

However, in the elastic case, higher thermal bowing is observed in comparison to the inelastic case during the later stages of fire exposure. This is attributed to additional eccentricity due to the fire induced material cracking. Figure 23 and Figure 24 show the overall thermo-mechanical response of the masonry walls at t=5 min and t=240 min, respectively. Upon exposure to fire, highly nonlinear thermal gradients are induced on to the structure and eventually, the presence of such nonlinear thermal gradients coupled with the mechanical load will result in the overall thermal expansion of the wall. However, as discussed in the case of half-scale masonry wall subjected to fire, the thermal expansion in the heated zone results in tension in the adjacent non-heated zone of the structure and eventually culminate into compressive stress in the heated zone. This phenomenon can be seen in Figure 23 (t=5 min) where the σ_{yy} at the exposed face is in compression, whereas the adjacent core to the exposed face is in tension. However, the stress states in the masonry wall are transient in nature due to nonlinear thermal gradients coupled with temperature-dependent material degradation and eventually severe cracking is observed in the wall at t=240 min (Figure 24, Normal cracking stress). The further explanation pertaining to such thermo-mechanics in the context of the present wall is provided with the aid of RVU-1 (Figure 25) and RVU-2 (Figure 26) taken at 1 m and 0 m heights from the base, respectively. The stress (σ_{yy}) histories at the designated locations, M_A, M_B and M_C (see Figure 23) in the considered RVUs are shown in Figure 27. In the case of RVU-1, the heated zone is under compression followed by tension in the adjacent cold zone (Figure 25, σ_{yy} at t=5 min). However, as time progresses, the aforementioned compression-tension zone transits over the wall thickness (Figure 25, σ_{yy} at t= 60 & 120 min) due to which, cracking is observed in the mortar (Figure 25, Normal cracking stress) which is relatively weaker compared to the brick units. These effects can be seen in the stress history plots as well (Figure 27, RVU-1, M_A &M_B). Moreover, after further fire exposure, a reduction in the compressive stress is observed in the heated zone, whereas reduction in tensile stress is observed in the adjacent non-heated zone (Figure 27, RVU-1, M_A &M_B).

This is mainly due to two thermo-mechanical phenomena. Firstly, change in the nature of nonlinear thermal gradients attributed to the cross-sectional heat diffusion. Secondly, due to the predominance of the material degradation over thermal dilation in the development of the thermal stresses. It should be mentioned that the discontinuity in stress profiles are observed at the brick-mortar interface (Figure 25, σ_{yy}), unlike the earlier half-scale wall due to the additional stresses generated due to the differential thermal expansion between the brick and mortar. For instance, for the chosen material properties, thermal increment of 1000 °C attributes to a differential thermal strain of 0.00066 which is significant enough to cause additional stresses.

Moreover, such stresses have resulted in vertical cracking (see Figure 25, normal cracking stress at t=120 and 240 min) in brick and mortar in the hot and cold zones, respectively. In the case of RVU-2 as well, above mentioned thermo-mechanical phenomena were observed with quantitatively similar stress (Figure 27, RVU-2) histories to that of RVU-1, with additional stresses and cracking zones attributing to the base restraint effects. Lastly, for the full-scale masonry wall under consideration, no failure was observed from the numerical simulation, both in terms of strength as well as the insulation failure criteria for the 240 min one-sided fire exposure.

5 Conclusions

A 2-D FE based simulation framework has been developed for thermo-mechanical analysis of solid brick masonry walls. The developed framework modelled unit and mortar separately, and accounted for geometric and material nonlinearities, transient states of strain and temperature-dependent material properties. The developed framework was considered validated as the thermo-mechanical predictions of half-scale masonry wall subjected to fire and the predictions were reasonably accurate, as compared to the experimental results. Utilizing the developed framework, thermo-mechanical analysis was performed on a full-scale masonry wall subjected to one-sided fire exposure.

Critical phenomena which included heat diffusion, nonlinear thermal gradients, unit-mortar thermo-mechanical interaction, cracking and stress profiles within the masonry structure were studied in detail in the above mentioned numerical investigations. Also, thermo-mechanics within a representative volume of unit and mortar at various locations were studied. Such unit level thermo-mechanics studies within the present numerical investigation have indicated the following insights. In both the walls, influence of boundary conditions was observed on the stress histories in the representative volume units. In case of the half-scale wall, extensive cracking and crushing in the masonry wall, especially near the base had resulted in the change in the kinematic equilibrium of the global structure and eventually culminated to the failure of the structure. In case of the full-scale clay brick masonry wall, progressive cracking was observed over time. However, no failure was observed in the numerical simulation for the given fire exposure, which was taken from the fire resistance ratings tabulated in EN1996-1-2. Moreover, the differential thermal expansion between the constituent materials of the masonry walls has resulted in additional stresses at the unit-mortar joint, and eventually resulted in vertical cracking profiles near the joints. Lastly, the developed 2-D FE simulation framework and subsequent detailed thermo-mechanical response history characterization demonstrated in the present study facilitates wide range of numerical applications pertaining to masonry structures. They include a) performance based structural fire design, b) sensitivity analysis, c) post-fire residual capacity assessment studies, and d) development of simplified empirical models.

6 Acknowledgements

The first author would like to acknowledge the post-doctoral fellowship offered by the University of Minho for this research. Funding provided by the Portuguese Foundation for Science and Technology (FCT) to the Research Project IntegraCrete (PTDC/ECM-EST/1056/2014 - POCI-01-

0145-FEDER-016841) is gratefully acknowledged. This work was financially supported by UID/ECI/04029/2019 - ISISE, funded by national funds through the FCT/MCTES (PIDDAC).

7 References

[1] P.B. Lourenço, G. Milani, A. Tralli, A. Zucchini, Analysis of masonry structures: Review of and recent trends in homogenization techniques, Can. J. Civ. Eng. 34 (2007) 1443–1457. https://doi.org/10.1139/L07-097.

[2] P.B. Lourenço, Computational strategies for masonry structures: multi-scale modeling, dynamics, engineering applications and other challenges, in: Congr. Métodos Numéricos En Ing., Semni, Bilbao, 2013: pp. 1–17.

[3] S. Russo, F. Sciarretta, Masonry exposed to high temperatures: Mechanical behaviour and properties—An overview, Fire Saf. J. 55 (2013) 69–86. https://doi.org/10.1016/j.firesaf.2012.10.001.

[4] European Committee for Standardization, EN 1996-1-2: Design of masonry structures - Part 1-2: General rules - Structural fire design, 2006.

[5] American Concrete Institute, ACI 216.1-07 / TMS-0216-07: Code Requirements for Determining Fire Resistance of Concrete and Masonry Construction Assemblies, 2007.

[6] M. Dhanasekaran, V. Chandrasekaran, S. Grubits, A numerical model for thermal bowing of masonry walls, in: 10th Int. Brick/Block Mason. Conf., Calgary, 1994.

[7] A. Nadjai, M. O'Garra, F.A. Ali, D.L.-F. and materials, undefined 2003, A numerical model for the behaviour of masonry under elevated temperatures, Wiley Online Libr. (n.d.). https://onlinelibrary.wiley.com/doi/abs/10.1002/fam.824 (accessed March 15, 2019).

[8] S.M. Byrne, Fire resistance of load-bearing masonry walls, Fire Technol. 15 (1979) 180–188. https://doi.org/10.1007/BF01983196.

[9] S. Lawrence, N. Gnanakrishnan, The fire resistance of masonry walls-an overview, in: Natl. Struct. Eng. Conf., National conference publication (Institution of Engineers, Australia), Melbourne, 1987: pp. 431–437.

[10] T. Shields, D. O'Connor, G.W.H. Silcock, H.A. Donegan, Thermal bowing of a model brickwork panel, in: Int. Brick/Block Mason. Conf., Dublin, 1988: pp. 846–856.

[11] D. Laverty, A. Nadjai, D.J. O'connor, Modelling of thermo-structural response of concrete masonry walls subjected to fire, J. Appl. Fire Sci. 10 (2000) 3–19.

[12] T.-D. Nguyen, F. Meftah, Behavior of clay hollow-brick masonry walls during fire. Part 1: Experimental analysis, Fire Saf. J. 52 (2012) 55–64. https://doi.org/10.1016/J.F

IRESAF.2012.06.001.

[13] EN1996-1-2: Design of masonry structures. Part 1–2: General rules –Structural Fire Design. Commission of European Communities, Brussels, 2005.

[14] Beureu of Indian Standards, “Indian Code of Practice for fire safety of buildings(General): Details of Construction-Code of Practice.,” IS-1641, New Delhi, 1989.

[15] A. Nadjai, M. O’Garra, F. A. Ali, D. Laverty, A numerical model for the behaviour of masonry under elevated temperatures, Fire Mater. 27 (2003) 163–182.

[16] A. Nadjai, M. O’Garra, F. Ali, Finite element modelling of compartment masonry walls in fire, Comput. Struct. 81 (2003) 1923–1930. https://doi.org/10.1016/S0045-7949(03)00212-8.

[17] A. Nadjai, M. O’Gara, F. Ali, R. Jurgen, Compartment Masonry Walls in Fire Situations, Fire Technol. 42 (2006) 211–231. https://doi.org/10.1007/s10694-006-7509-6.

[18] T.-D. Nguyen, F. Meftah, Behavior of hollow clay brick masonry walls during fire. Part 2: 3D finite element modeling and spalling assessment, Fire Saf. J. 66 (2014) 35–45. https://doi.org/10.1016/J.FIRESAF.2013.08.017.

[19] P. Kumar, G. Srivastava, Effect of fire on in-plane and out-of-plane behavior of reinforced concrete frames with and without masonry infills, Constr. Build. Mater. 167 (2018) 82–95. https://doi.org/10.1016/J.CONBUILDMAT.2018.01.116.

[20] DIANA, DIANA User’s Manual Release 10.2, (2019).

[21] A. Mohyeddin-Kermani, Modelling and performance of RC frames with masonry infill under in-plane and out-of-plane loading, The University of Melbourne, 2011.

[22] Naus D J, The Effect of Elevated Temperature on Concrete Materials and Structures - A Literature Review, Oak Ridge National Laboratory, Oak Ridge, 2005.

[23] J. Argyris, J. Doltsinis, On the natural formulation and analysis of large deformation coupled thermomechanical problems, Comput. Methods Appl. Mech. Eng. 25 (1981) 195–253.

[24] R.D. Cook, D.S. Malkus, M.E. Plesha, R.J. Witt, Concepts and applications of finite element analysis, John Wiley & Sons, Newyork, 2007.

[25] G. Torelli, P. Mandal, M. Gillie, V.-X. Tran, Concrete strains under transient thermal conditions: A state-of-the-art review, Eng. Struct. 127 (2016) 172–188. https://doi.org/10.1016/J.ENGSTRUCT.2016.08.021.

[26] G. Srivastava, P.R. Prakash, An integrated framework for nonlinear analysis of plane frames exposed to fire using the direct stiffness method, Comput. Struct. 190 (2017) 173–185.

[27] Y. Anderberg, S. Thelandersson, Stress and deformation characteristics of concrete at high

temperatures. Experimental investigation and material behaviour model, Lund Institute of Technology, Lund University, Sweeden, 1976.

[28] R. Cope, P. Rao, L. Clark, P. Norris, Modeling of reinforced concrete behavior for finite element analysis of bridge slabs, in: Numer. Methods Non-Linear Probl., Pineridge Press, Swansea, 1980: pp. 457–470.

[29] J.G. Rots, Various crack concepts for curved fracture in concrete, in: Proc. 7th Int. Conf. Fract., Elsevier Ltd, Houston, 1989: pp. 2279–2287.

[30] H. Akbar, Cracking in reinforced concrete analysis, J. Struct. Eng. (United States). 110 (1984) 1735–1746. https://doi.org/10.1061/(ASCE)0733-9445(1984)110:8(1735).

[31] European Committee for Standardization, EN 1992-1-2: Design of concrete structures - Part 1-2: General rules - Structural fire design, 2004.

[32] M. Crisfield, Non-linear finite element analysis of solids and structures., 1st ed., Wiley, Newyork, 1993.

[33] International Fedaration for Structural Concrete, FIB Model Code for Concrete Structures, Ernst & Sohn, 2010.

[34] S. Thelandersson, Effect of High Temperatures on Tensile Strength of Concrete, Lund Institute of Technology, 1972.

[35] European Committee for Standardization, EN 1996-1-1: Design of masonry structures - Part 1-1: General rules for reinforced and unreinforced masonry structures, 2005.

[36] J. Brooks, Concrete and Masonry Movements, Elsevier, 2015.

[37] P.B. Lourenço, J. Almeida, J. Barros, Experimental investigation of bricks under uniaxial tensile testing, Mason. Int. 18 (2005) 11–20.

585 **Tables**

586

587 **Table 1: Physical properties of half-scale masonry wall subjected to fire (*T*= 20 °C).**

Physical property	Value
Geometry	See Figure 4
Applied load (kN)	50
Concrete unit:	
Compressive strength (MPa)	20
Tensile strength (MPa)	2
Poison's ratio	0.17
$\varepsilon_{cp,20}$	0.0023
$\varepsilon_{cu,20}$	0.005
Thermal expansion coefficient (/°C)	6×10^{-6} (Calcareous aggregates)
Heat capacity (kJ/m^{3}K)	2100
Thermal Conductivity (W/mK)	1.36
Mortar joint:	
Compressive strength (MPa)	10
Tensile strength (MPa)	1
Poison's ratio	0.2
$\varepsilon_{cp,20}$	0.004
$\varepsilon_{cu,20}$	0.009
Thermal expansion coefficient (/°C)	6×10^{-6} (Calcareous aggregates)
Heat capacity (kJ/m^{3}K)	2100
Thermal Conductivity (W/mK)	1.36

588

589

Table 2: Physical properties of full-scale masonry wall subjected to fire.

Physical property	Value
Geometry	See Figure 18
Applied load (MPa)	0.8538
Clay unit:	
Compressive strength (MPa)	30
Tensile strength (MPa)	3
Poison's ratio	0.17
$\varepsilon_{cp,20}$	0.00175
$\varepsilon_{cu,20}$	0.0019
Thermal expansion coefficient (/°C)	5.33×10^{-6} (Clay units)
Heat capacity (kJ/m^{3}K)	676
Thermal Conductivity (W/mK)	0.42
mode-1 fracture energy (N/m)	55
Mortar joint:	
Compressive strength (MPa)	10
Tensile strength (MPa)	1
Poison's ratio	0.2
$\varepsilon_{cp,20}$	0.0025
$\varepsilon_{cu,20}$	0.02
Thermal expansion coefficient (/°C)	6×10^{-6} (Calcareous aggregates)
Heat capacity (kJ/m^{3}K)	2100
Thermal Conductivity (W/mK)	1.36

Figures

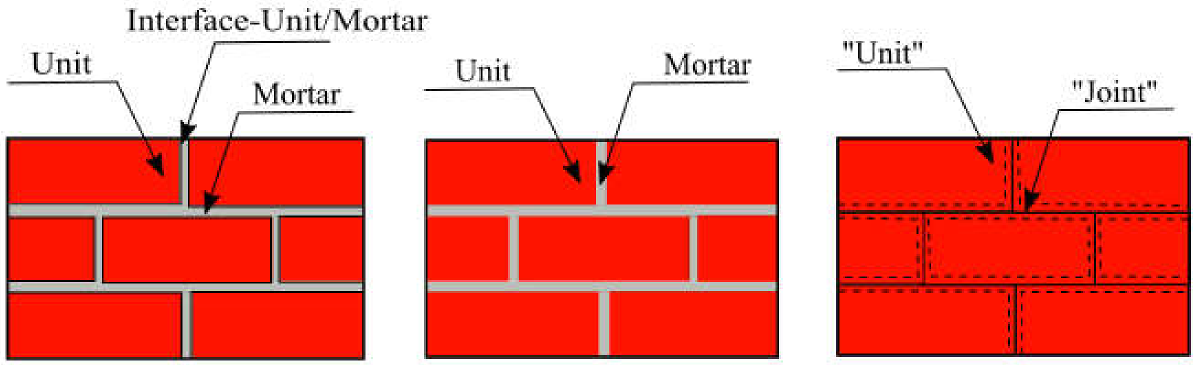

a) Detailed Micro model b) Continum Micro model c) Simplified Micro model

Figure 1: Micro modelling strategies in masonry [2].

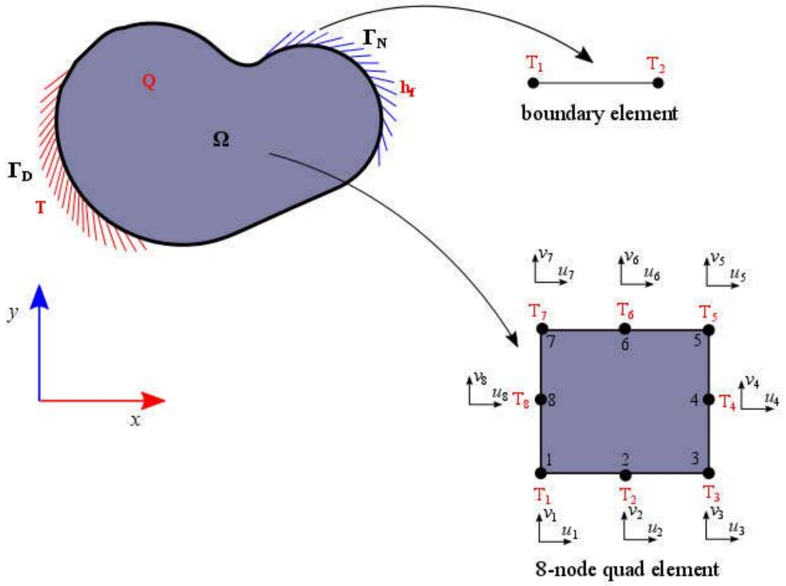

Figure 2: 2-D Thermo-mechanical modelling and discretization strategy.

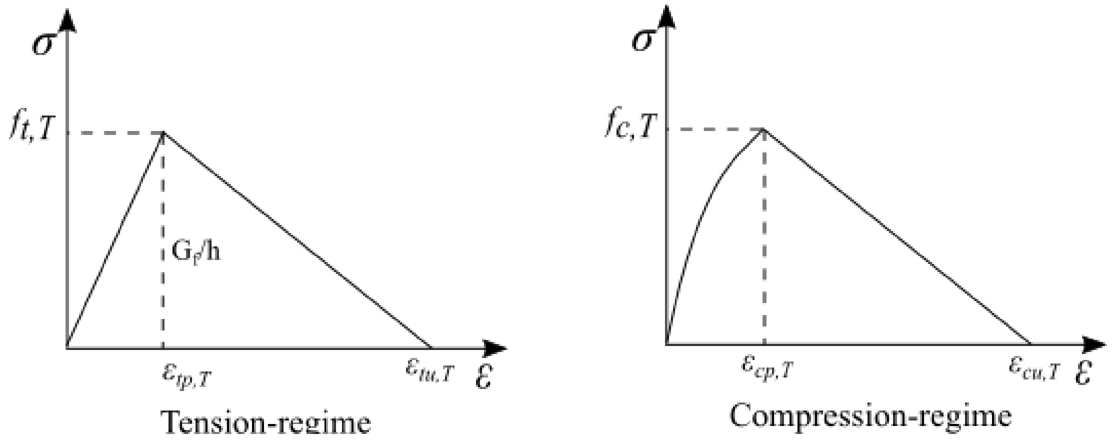

Figure 3: 1-D tension and compression constitutive behavior used in the total-strain rotating crack model.

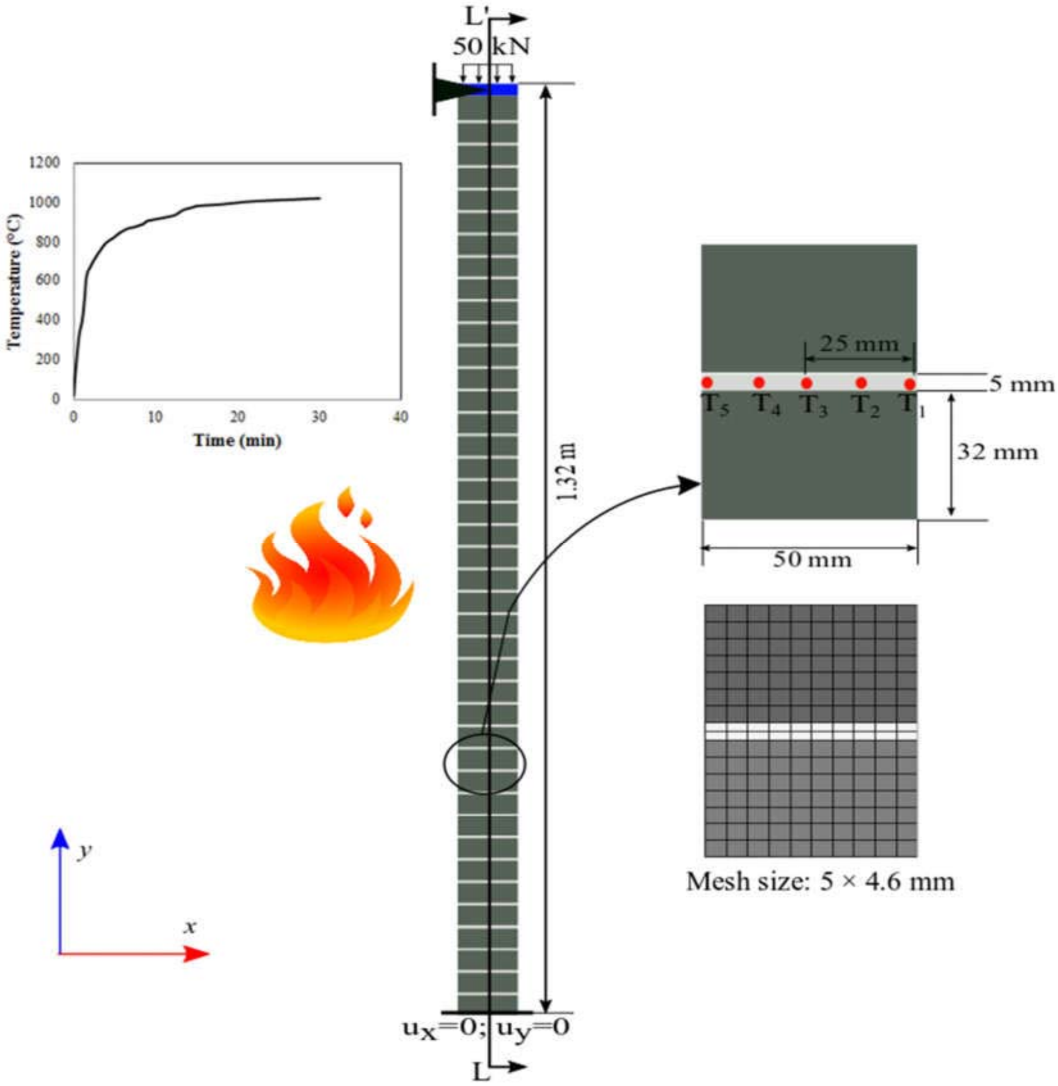

Figure 4: Half-scaled masonry wall subjected to fire.

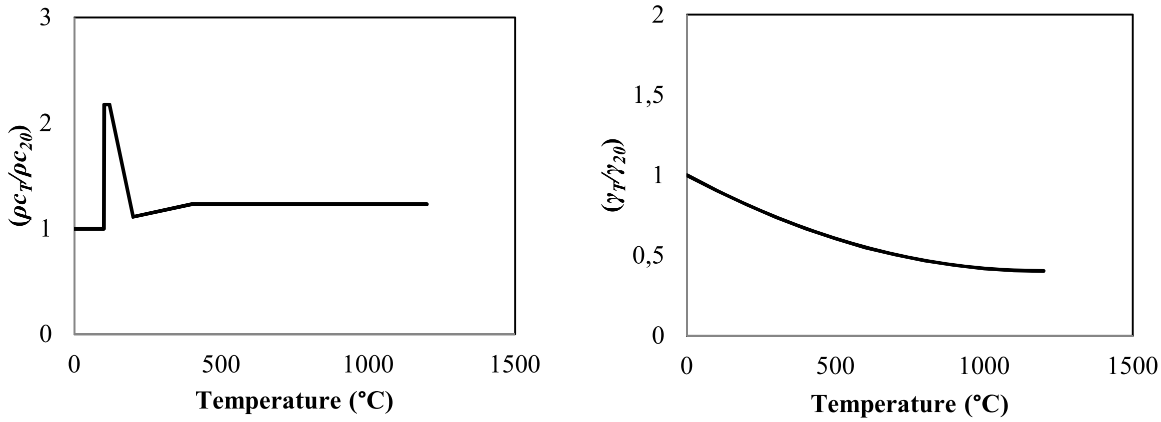

a) Specific-heat capacity

b) Thermal-conductivity

Figure 5: Temperature-dependent thermal properties of concrete unit and cement mortar.

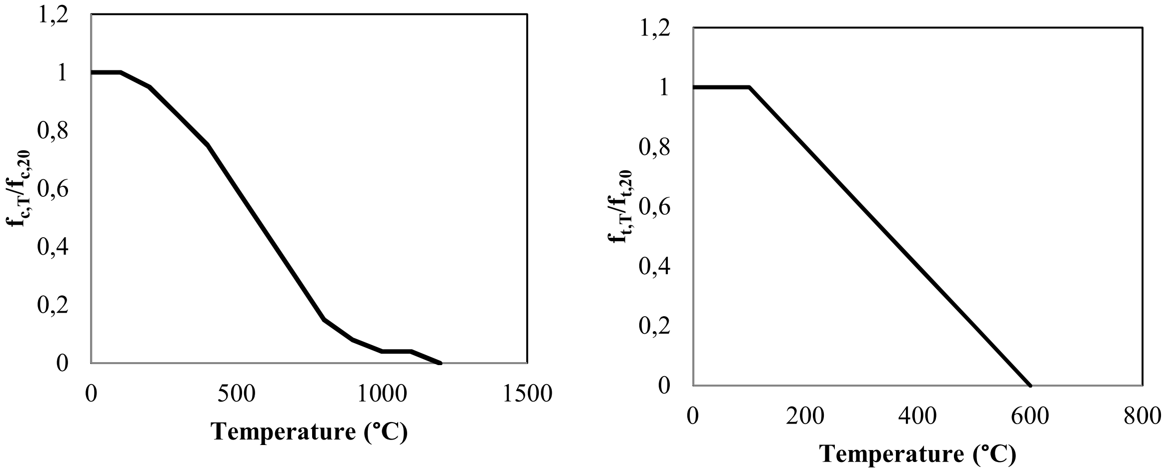

a) Compressive strength ($f_{c,T}$) b) Tensile strength ($f_{t,T}$)

Figure 6: Temperature-dependent compressive and tensile strengths of concrete unit and cement mortar.

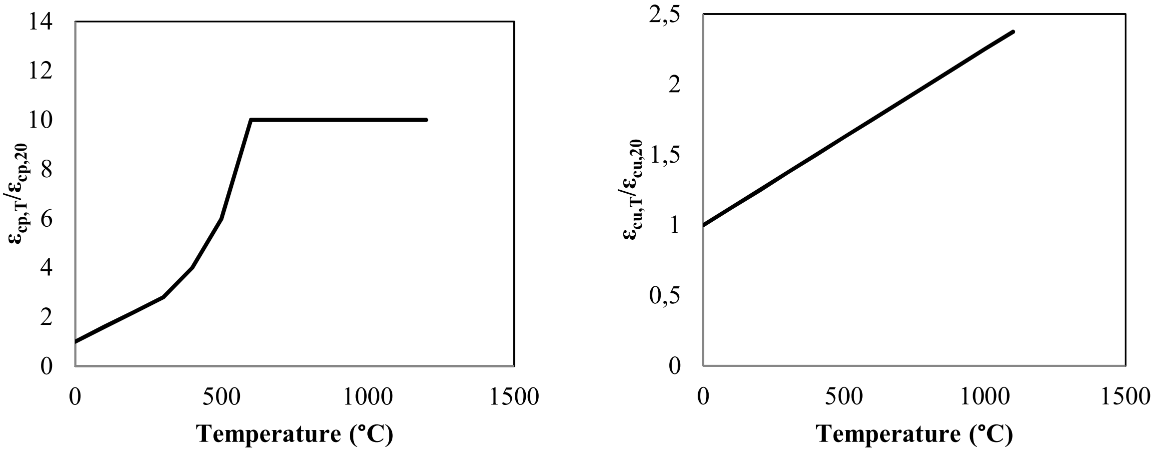

a) Strain at peak compressive strength ($\varepsilon_{cp,T}$) b) Ultimate compressive strain ($\varepsilon_{cu,T}$)

Figure 7: Temperature-dependent $\varepsilon_{cp,T}$ and $\varepsilon_{cu,T}$ of concrete unit and cement mortar.

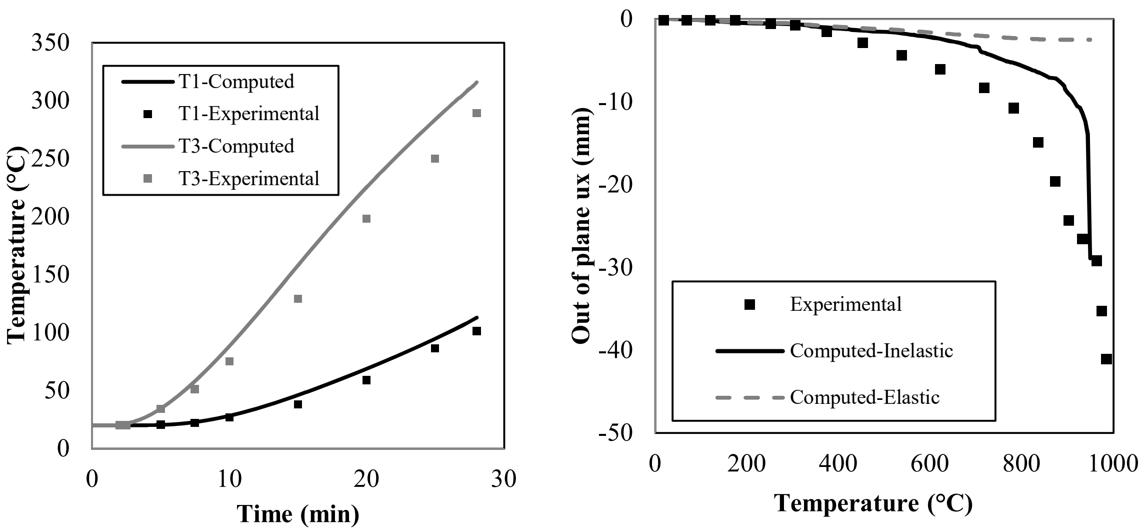

a) Temperature b) Out of plane deflection

Figure 8: Comparison of experimental and computed response.

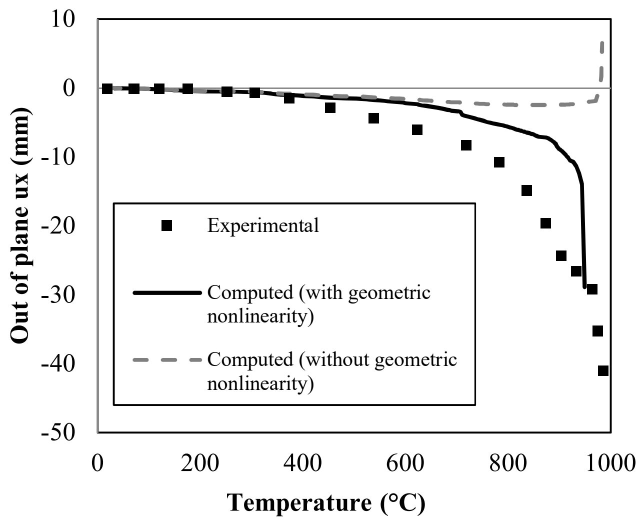

Figure 9: Effect of geometric nonlinearity on the thermo-mechanical response of the half-scale wall.

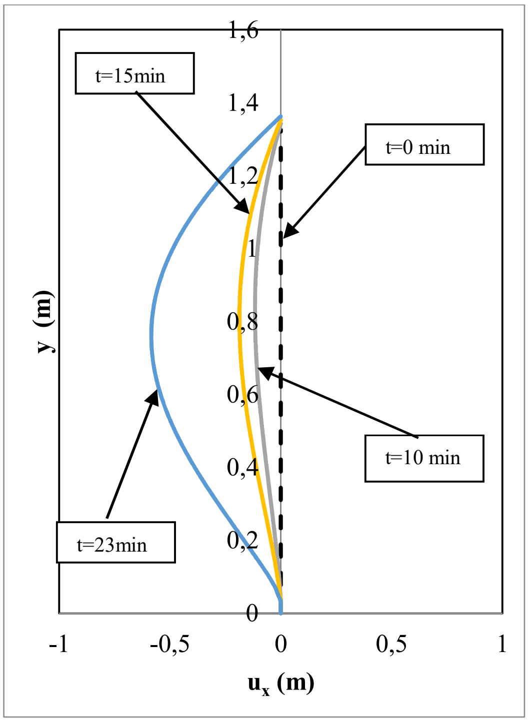

Figure 10: Deformed configuration of the central line of the half-scale wall (Scaling 30x)

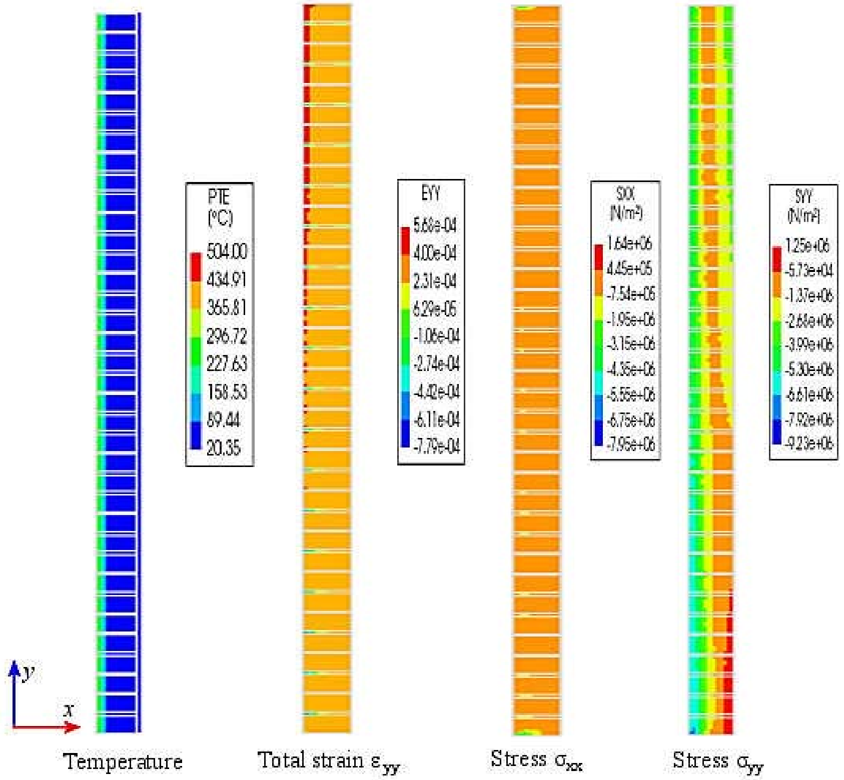

Figure 11: Thermo-mechanical response of half-scale masonry wall at t=5 min.

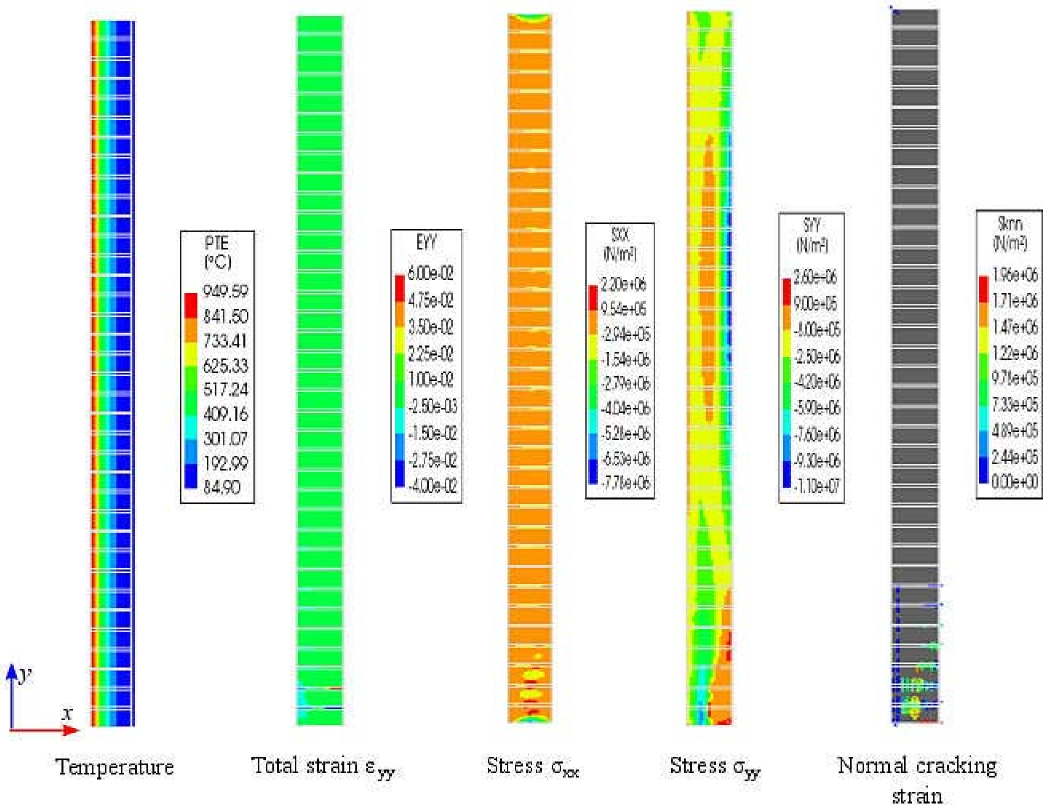

Figure 12: Thermo-mechanical response of half-scale masonry wall at t=23 min.

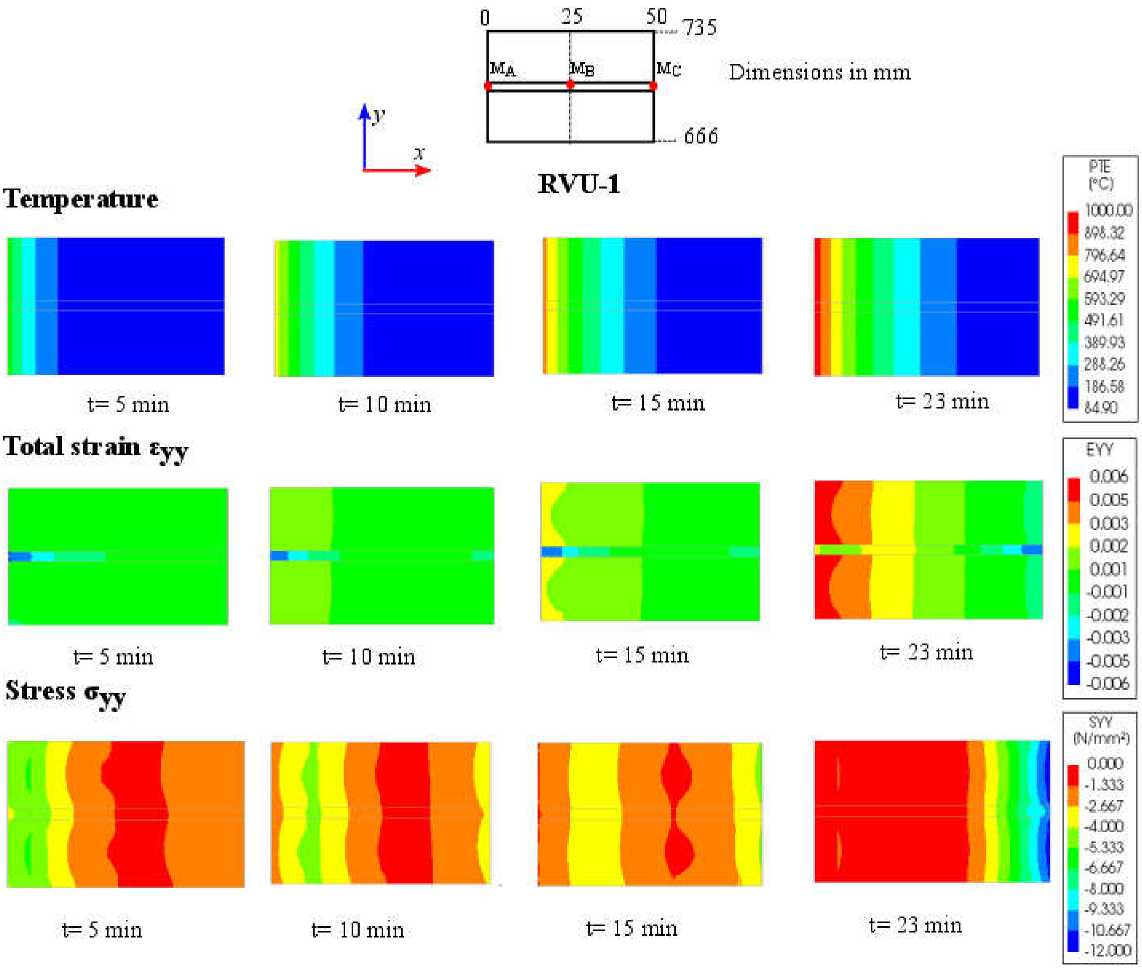

Figure 13: Thermo-mechanical response history of RVU-1 (half-scale masonry wall at 0.66 m from base).

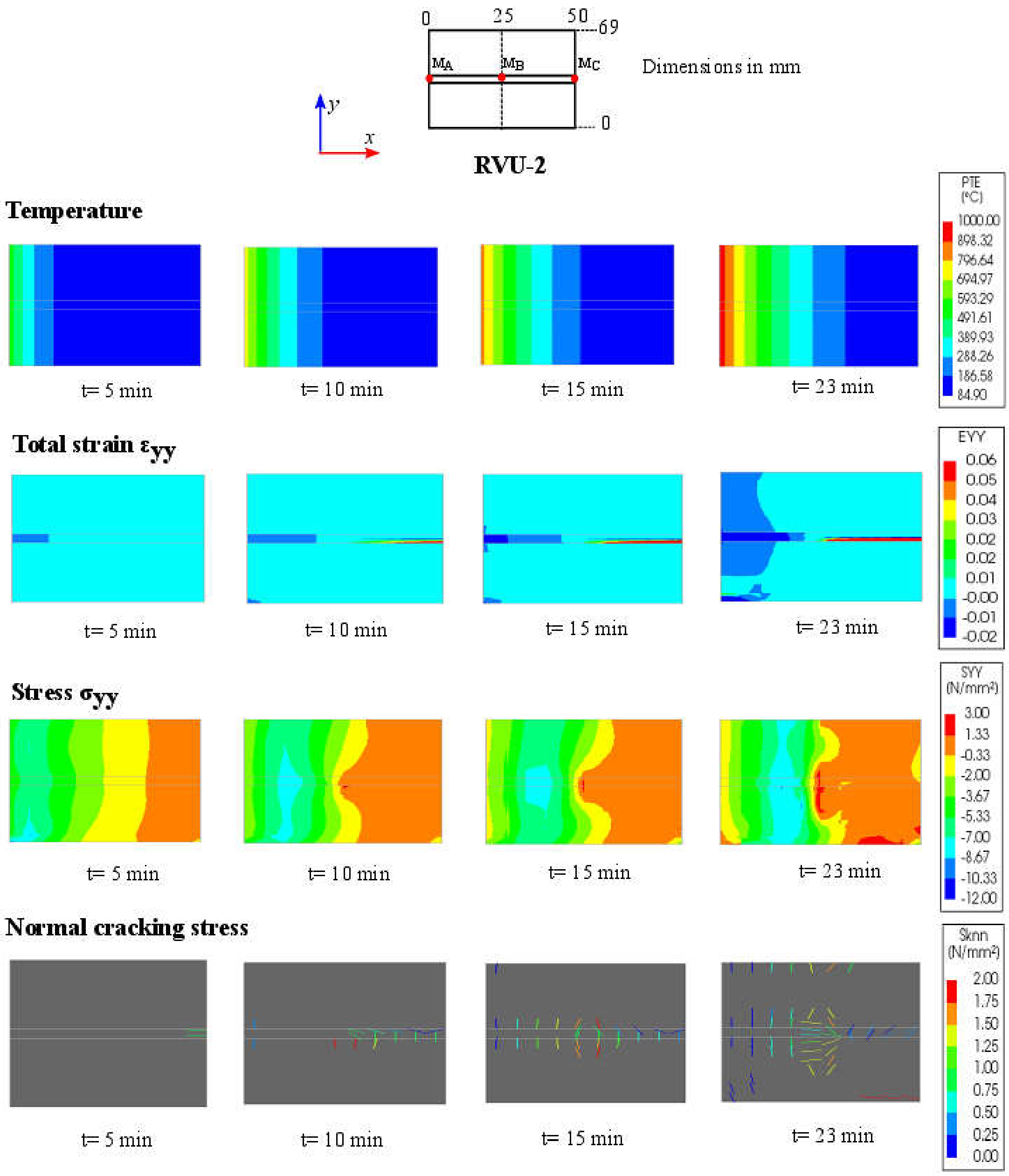

Figure 14: Thermo-mechanical response history of RVU-2 (half-scale masonry wall at 0 m form base).

653

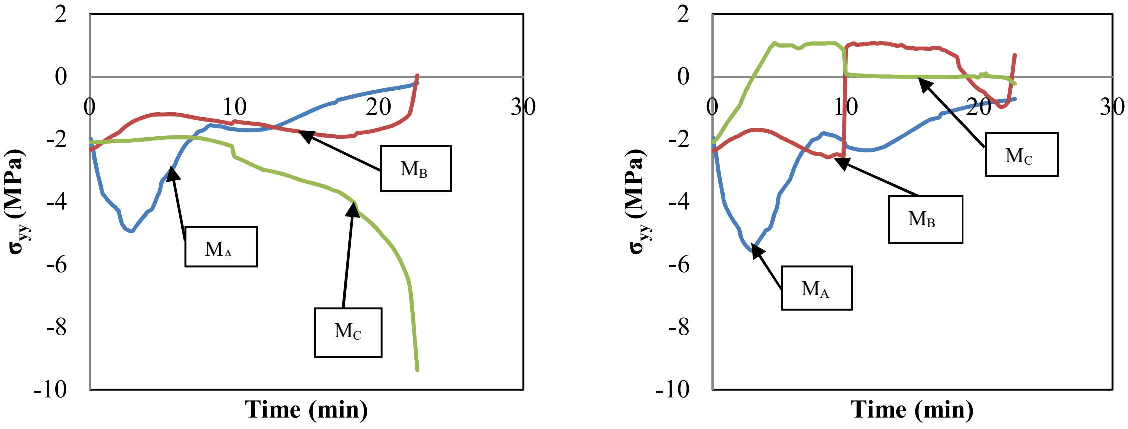

a) RVU-1 b) RVU-2

654 **Figure 15: Stress states in RVU-1 and RVU-2 of the half-scale masonry wall.**

655

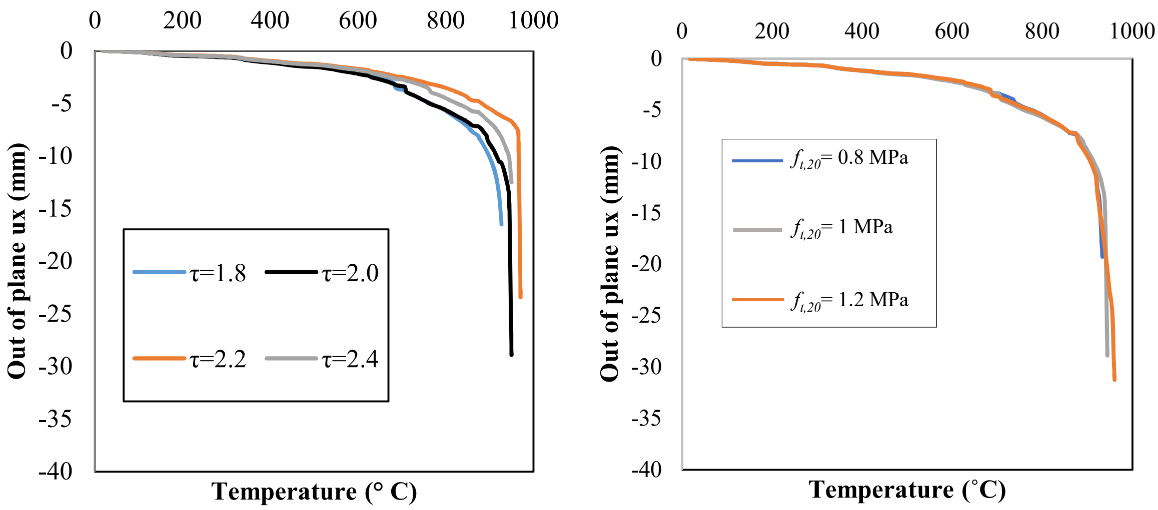

a) Effect of Transient creep b) Effect of tensile strength of mortar

Figure 16: Parametric studies on transient creep and tensile strength of mortar.

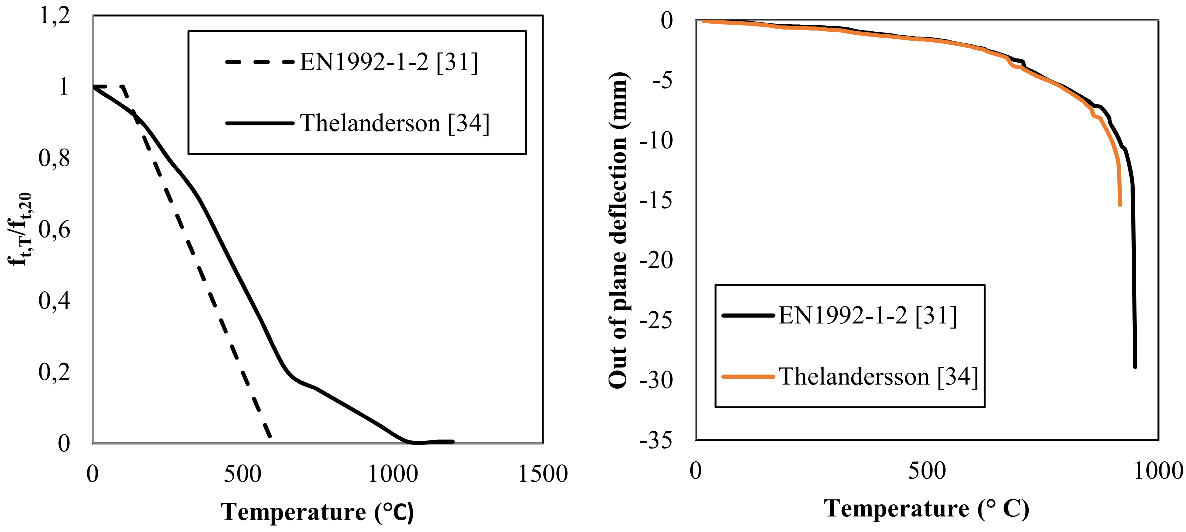

a) Temperature-dependency in tensile strength

b) Effect of temperature-dependency in concrete unit and cement mortar

Figure 17: Parametric studies on temperature-dependency of concrete unit and cement mortar.

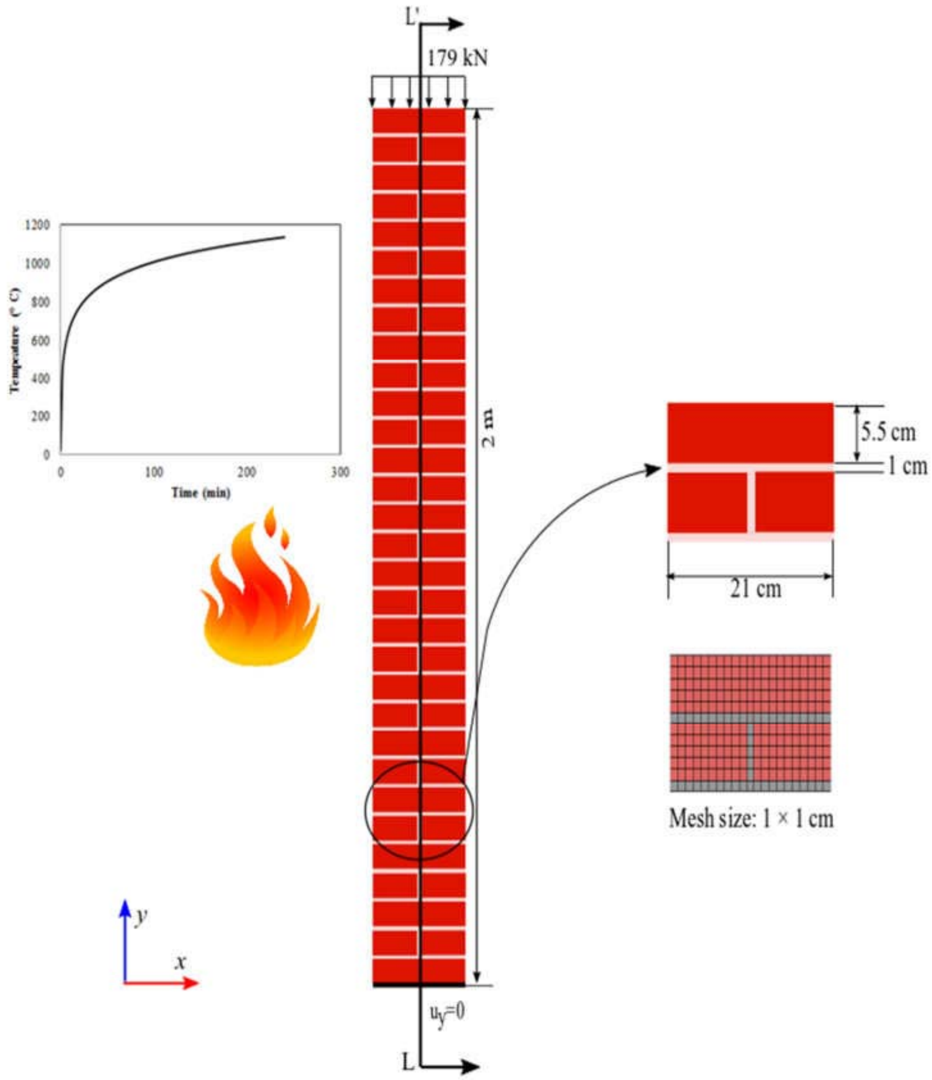

Figure 18: Full-scale masonry wall subjected to standard fire exposure.

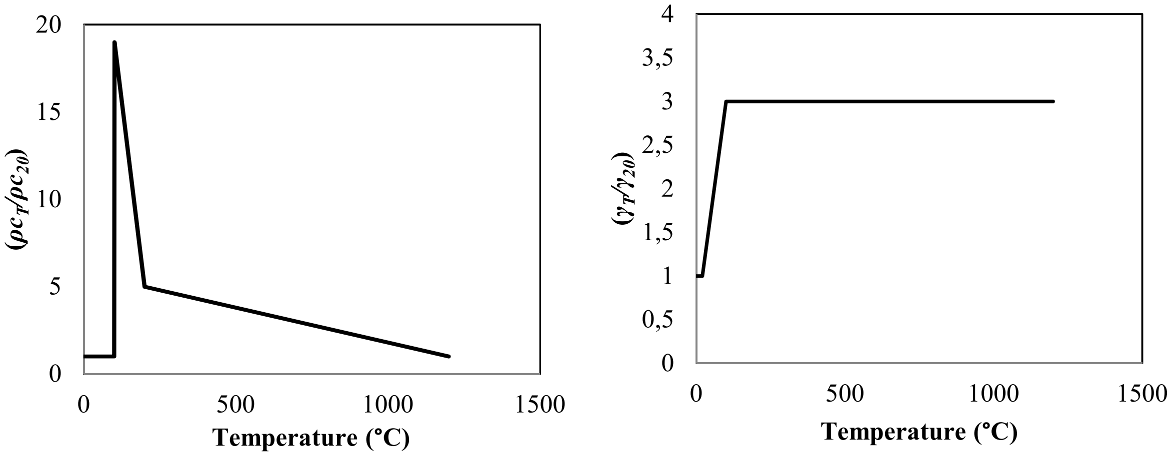

a) Specific-heat capacity b) Thermal-conductivity

Figure 19: Temperature-dependent thermal properties of clay unit.

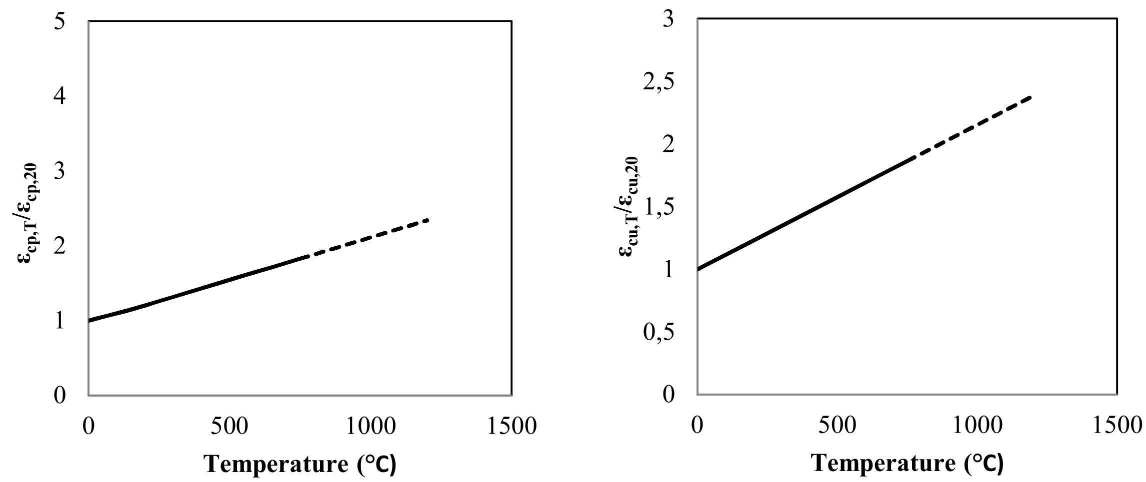

a) Strain at peak compressive strength ($\varepsilon_{cp,T}$) b) Ultimate compressive strain ($\varepsilon_{cu,T}$)

Figure 20: Temperature-dependent $\varepsilon_{cp,T}$ and $\varepsilon_{cu,T}$ in clay unit.

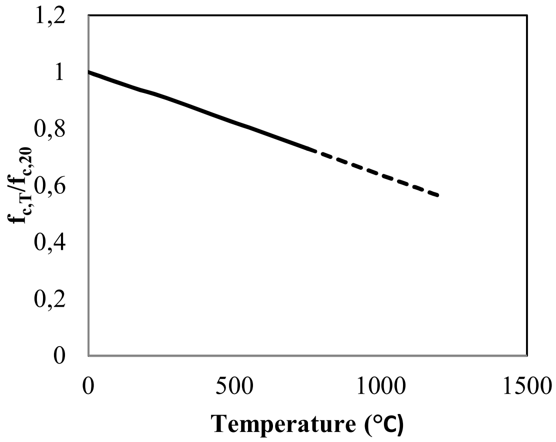

Figure 21: Temperature-dependent compressive strength of clay unit.

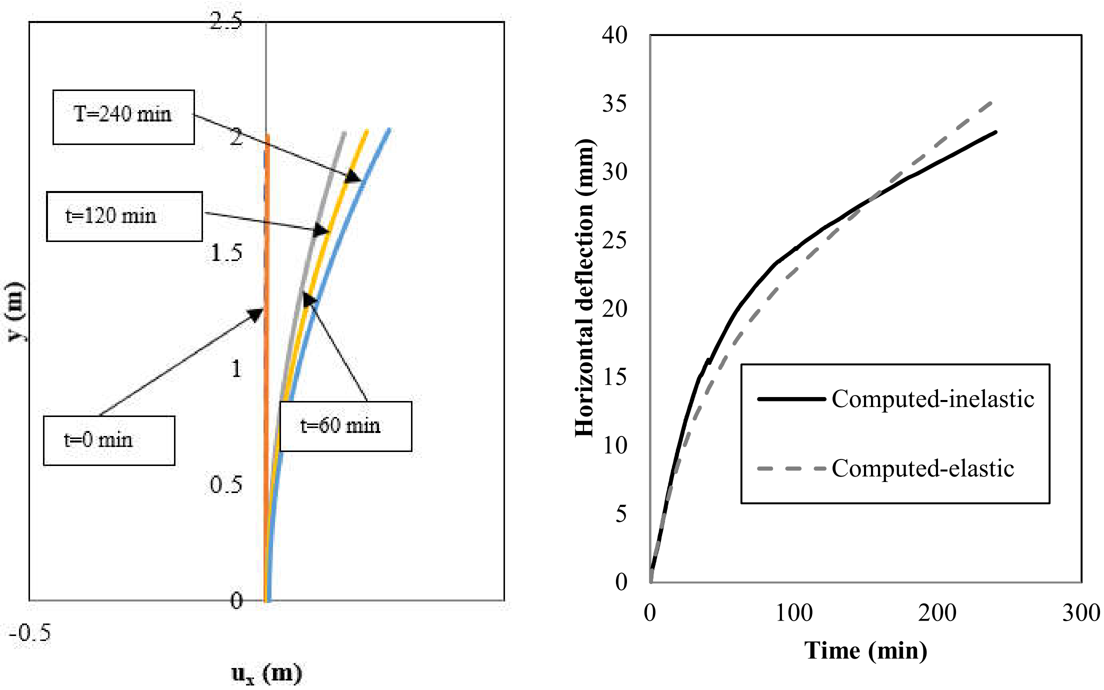

a) Deformed configuration of the central line

b) Deformation history at the top of the masonry wall

Figure 22: Deformed mechanical response of full-scale wall (Scaling 10x).

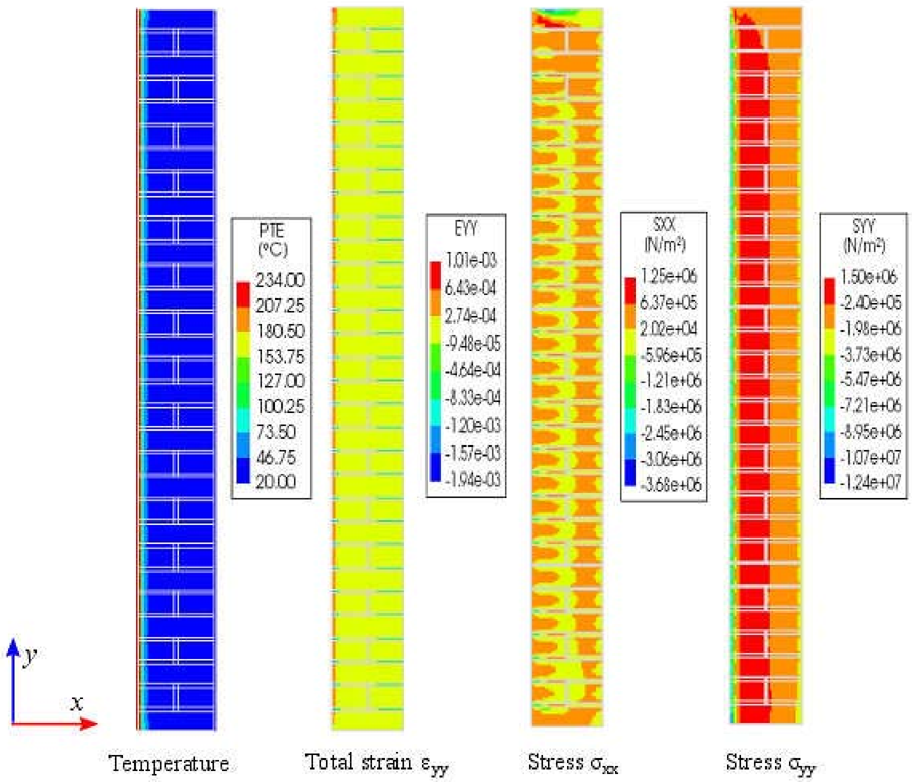

Figure 23: Thermo-mechanical response of full-scale masonry wall at t=5 min.

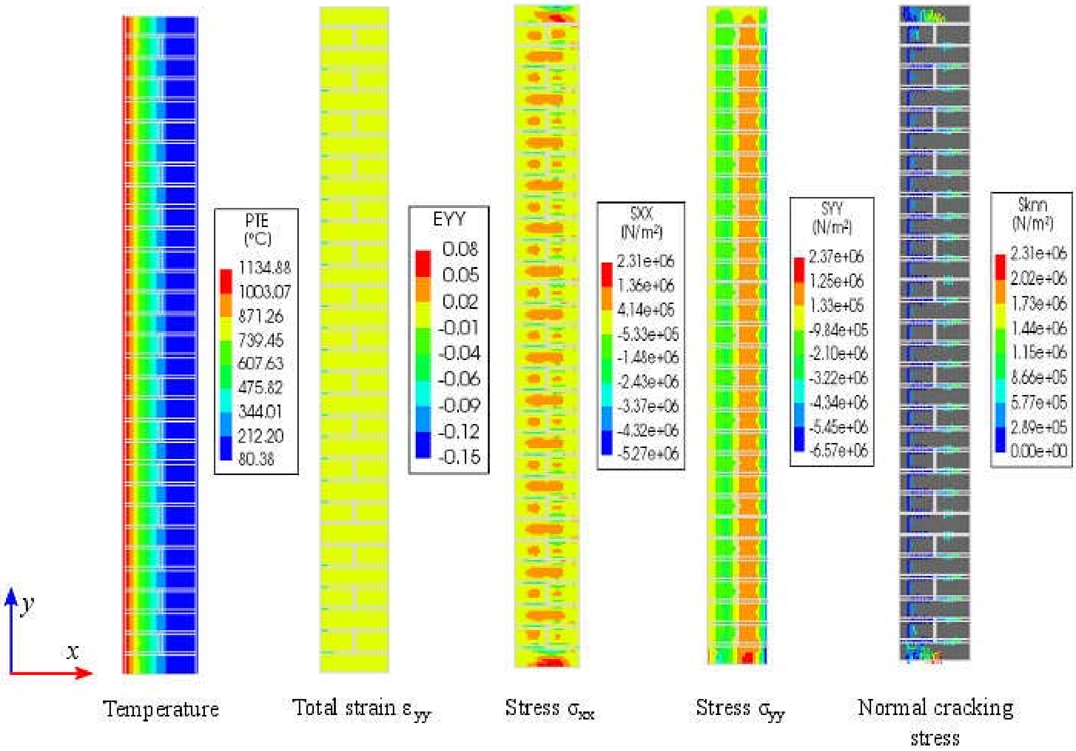

Figure 24: Thermo-mechanical response of full-scale masonry wall at t=240 min.

Preprint version, Reference: Patnayakuni RP, Azenha M, Pereira JM, Lourenço PB (2020), Finite element based micro modelling of masonry walls subjected to fire exposure: framework validation and structural implications. Engineering Structures, 213, 110545. https://doi.org/10.1016/j.engstruct.2020.110545

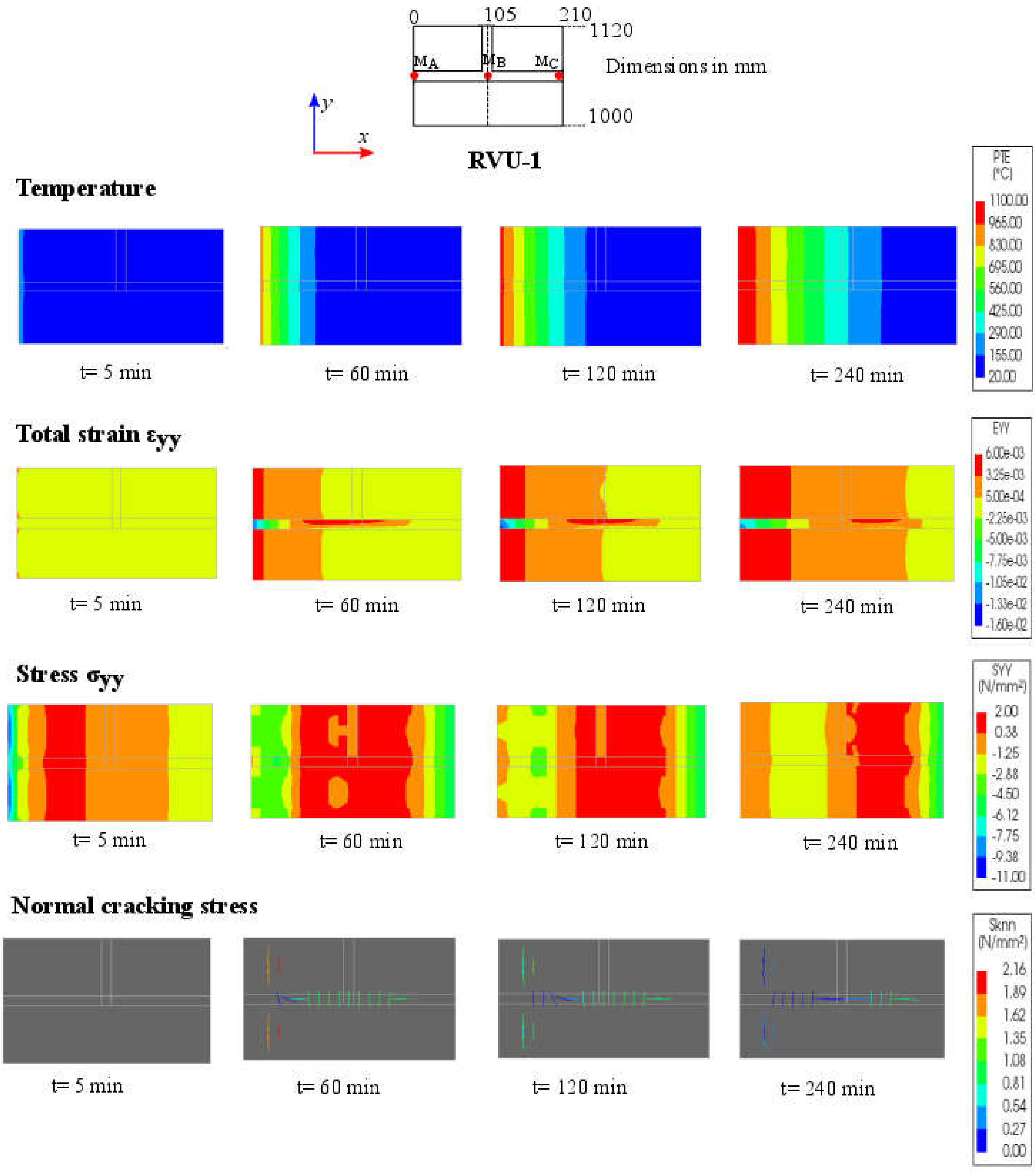

Figure 25: Thermo-mechanical response history of RVU-1 (full-scale masonry wall at 1 m from base).

693

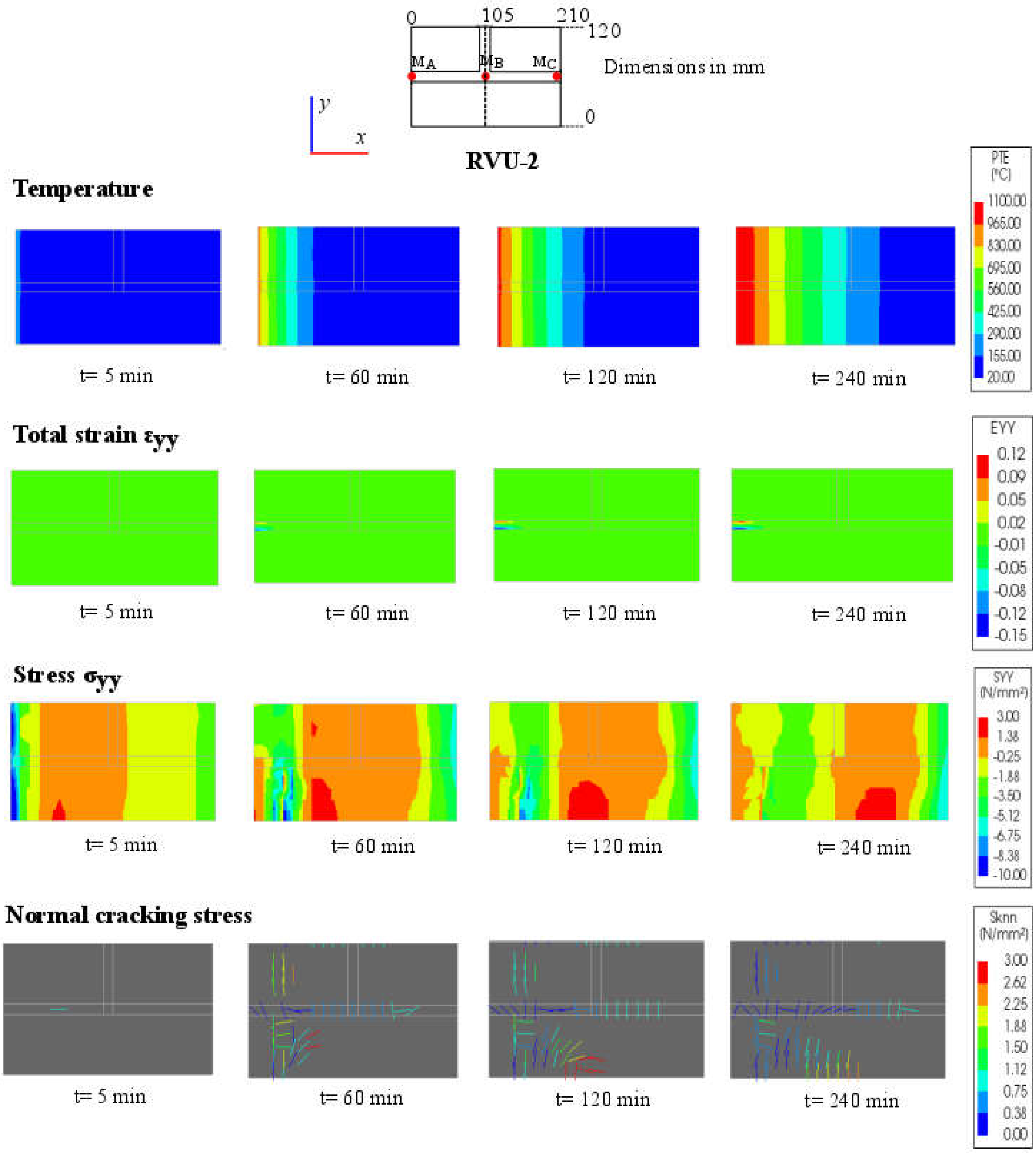

694

695 **Figure 26: Thermo-mechanical response history of RVU-2 (full-scale masonry wall at 0 m**

696 **from base).**

697

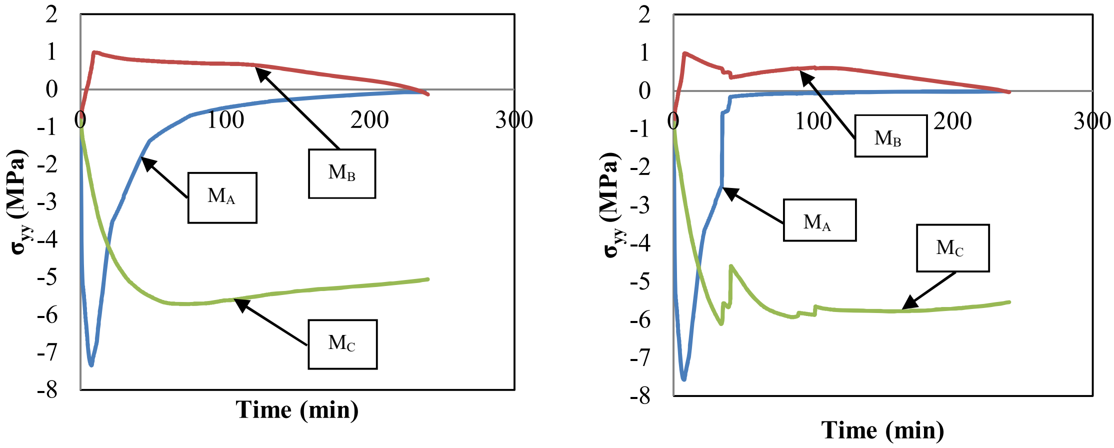

a) RVU-1 b) RVU-2

Figure 27: Stress states in RVU-1 and RVU-2 of the full-scale masonry wall.